

The Radiation Pattern and Phase Center of Two-Dimensional Apertures

Khadija Embais

Submitted to the
Institute of Graduate Studies and Research
in partial fulfillment of the requirements for the degree of

Master of Science
in
Electrical and Electronic Engineering

Eastern Mediterranean University
February 2016
Gazimağusa, North Cyprus

Approval of the Institute of Graduate Studies and Research

Prof. Dr. Cem Tanova
Acting Director

I certify that this thesis satisfies the requirements as a thesis for the degree of Master of Science in Electrical and Electronic Engineering.

Prof. Dr. Hasan Demirel
Chair, Department of Electrical and
Electronic Engineering

We certify that we have read this thesis and that in our opinion it is fully adequate in scope and quality as a thesis for the degree of Master of Science in Electrical and Electronic Engineering.

Asst. Prof. Dr. Rasime Uygurođlu
Supervisor

Examining Committee

1. Prof. Dr. Hasan Demirel

2. Prof. Dr. Abdullah Öztoprak

3. Assoc. Prof. Dr. Rasime Uygurođlu

ABSTRACT

Two matching techniques namely linearly tapered and multistep transition were used to design two dimensional radiators between parallel plate regions and 50Ω microstrip feed line. Transitions for different aperture widths were designed at 2.45GHz, by using a full wave simulation software.

As these radiators are not point radiators, they may cause phase errors. In this study, a simple method is suggested to estimate the phase center of the radiating apertures and reduce the phase errors. The suggested method is based on the phase equally in the broadside direction and at another constant angle. The study has been carried out by using a full wave simulation software.

The results show that there is almost no phase error over the range of angles of interest for the estimated phase center at the design frequency. The position of the phase does not vary with the distance from the radiator, which means that there are no phase errors as the distance from the radiator varies. Although there is some phase errors as the frequency is decreased or increased, these errors are not significant over a wide band of frequencies. For the multistep transition it is observed that the position of the phase center is closer to the center of the radiator aperture, for the wide apertures.

Keyword: Phase center, parallel plate, two dimensional radiation, far field region

ÖZ

İki uyumlaştırma yöntemi kullanılarak (çok aşamalı geçiş ve doğrusal değişimli geçiş), 50Ω mikroşerit besleme hattı ile paralel levhalardan oluşan bölge arasında antenler tasarlanmıştır. Tam dalga benzetim yazılımı kullanılarak, farklı açıklıklardaki, iki boyutlu antenlerin mikroşerit iletim hattı ile 2.24GHz tasarım frekansında uyumlaştırılması için çalışma yapılmıştır.

Belli açıklıkları olan bu antenler isotropik özelliğe sahip olmadığı için, faz hataları oluşmaktadır. Bu çalışmada, faz hatalarını azaltmayı hedefleyen, iki boyutlu antenlerin faz merkezini belirlemek için geliştirilen bir yöntem tanıtılmaktadır. Bu yöntem, uzak alanda, anten açıklık merkezi referans noktasından ölçülen açıya karşı oluşan faz hataları kullanılarak geliştirilmiştir. Faz merkezi, antene dik olan açı ile seçilen başka bir açıdaki fazları eşitleyerek elde edilmiştir.

Yapılan çalışmanın sonuçları, tasarım frekansında ilgili açılarda, hemen hemen hiç faz hatası bulunmadığını göstermektedir. Faz merkezinin konumu antenden olan mesafe ile değişmemektedir ki bu da, faz hatalarının antenden olan uzaklıkla değişmediği anlamına gelmektedir. Frekansın değişimi ile bazı faz hataları gözlemlenmekle beraber, bu hatalar geniş bir frekans bandına göre önem arz etmemektedir. Çok aşamalı geçiş için faz merkezi konumu, geniş açıklıklar için, antenin açıklık merkezine daha yakın olduğu gözlenmektedir.

Anahtar Kelimeler: faz merkezi, paralel iletken levha, iki boyutlu radyasyon, uzak alan bölgesi.

DEDICATION

To my teacher in this live who teach me how to fight for my hopes? To the light that guided me to make my dreams' comes truth. To my largest lost in my live.

To My Mother

ACKNOWLEDGMENT

I would like to express my special thanks to my supervisor Asst. Prof. Dr. Rasime Uygurođlu for her continuous support and guidance in the preparation of this study. Without her invaluable supervision, all my efforts could have been short-sighted. Also I am grateful to Prof. Dr. Abdullah Y. Öztoprak for his his guidance supporting during the research time.

Assoc. Prof. Dr. Hasan Demird Chairman of the Department of Electrical and Electronic Engineering for his helping, advising and assistance during my study in Eastern Mediterranean University, North Cyprus and I am grateful to him.

I owe quit a lot to my sister and my brothers who allowed me to travel all the way from Libya to Cyprus and supported me all throughout my studies. I would like to dedicate this study to them as an indication of their significance in this study as well as in my life.

Finally, I cannot forget my friends to thank them for everything.

TABLE OF CONTENTS

ABSTRACT.....	iii
ÖZ.....	iv
DEDICATION.....	v
ACKNOWLEDGMENT.....	vi
LIST OF TABLES.....	ix
LIST OF FIGURES.....	x
LIST OF SYMBOLS AND ABBREVIATIONS.....	xiii
1 INTRODUCTION.....	1
1.1 Introduction.....	1
1.2 Thesis Objectives.....	3
1.3 Thesis Contribution.....	4
1.4 Thesis Organization.....	4
2 MATCHING THECHNIQUES.....	5
2.1 Matching Overview.....	5
2.2 Rotman Lens Overview.....	6
2.3 Linearly Tapered Model.....	7
2.4 Stepped Transition Model.....	9
2.4.1 Rotman Lens as a Parallel Plate Region.....	9
2.4.2 Standing Wave Pattern.....	10
2.4.3 Multi-Section Transition.....	13
2.4.4 The Simulation Results of the Multi-sections Design.....	14
3 THE PHASE CENTER POSTION.....	23

3.1 Determination of The Phase Center.....	23
3.1.1 Electrical Field Radiated by the Multi-section transition.....	32
3.2 Phase Center Estimation.....	25
3.3 The Phase Center Simulation Result... ..	28
3.3.1 Phase Center of The Multi-sections Transitions.....	28
3.3.2 Phase Center of The Linear Taper.....	33
4 CONCLUSION AND FUTURE WORK.....	43
4.1 Conclusions.....	43
4.2 Future Work.....	43

LIST OF TABLES

Table 2.1: Parameters Design of Parallel plate	7
Table 2.2: Design Parameters of the Parallel plate Structure.....	14
Table 2.3: The Values and the Dimensions of the Three Multi-section Parameters Design.....	20
Table 3.1: The Values of Parameters of the Phase Center Position of Multi-Section	30
Table 3.2: The Values of Parameters of the Phase Center Position of Linear Taper	34
Table 3.3: Comparison of the phase center position for multi-section and linear taper transitions.....	39

LIST OF FIGURES

Figure 1.1: Rotman lens geometric design.....	2
Figure 2.1: Matching circuit diagram.....	5
Figure 2.2: Trifocal lens design scheme.....	6
Figure 2.3: Microstrip rotman lens design.....	8
Figure 2.4: Full wave simulation software model of linear taper transition.....	8
Figure 2.5: Parameter relationship for the linear taper design	9
Figure 2.6: Parallel plate region connected with microstrip line.....	10
Figure 2.7: Standing wave pattern curve.....	10
Figure 2.8: Microwstrip line parameters.....	12
Figure 2.9: Three multi-sections transition.....	13
Figure 2.10: 17.78mm aperture width with a microstrip feeding line.....	14
Figure 2.11: Standing wave pattern of 17.78mm aperture.....	15
Figure 2.12: Section A and section B.....	16
Figure 2.13: Standing wave pattern for connecting section B to section A.....	17
Figure 2.14: Final multi-section design.....	17
Figure 2.15: The dimension of multi-sections design.....	18
Figure 2.16: The return loss curve for multi-section transition (17.78mm).....	18
Figure 2.17: Linearly tapered between 50Ω line and the parallel plate region	19
Figure 2.18: Comparison S11 between linear tapered and multi-sections transition..	19

Figure 2.19: Multi-section and linearly tapered designs.....	21
Figure 2.20: Return loss curves for multi-section and linear taper transitions ($W_A = \frac{\lambda}{2}$)	21
Figure 2.21: Return loss for multi-section and linear taper transitions ($W_A = \frac{3\lambda}{4}$).....	22
Figure 3.1: The electric field Intensity of multi-section transition below the Parallel... Plate region for $W_A = 17.78\text{mm}$	24
Figure 3.2: The electric field Intensity of wide aperture below the parallel plate region for $W_A = 58.38\text{mm}$	25
Figure 3.3: Radiation patten at $R=2.8\lambda$ for $W_A = 17.78\text{mm}$ aperture width.....	25
Figure 3.4: The phase error between $\theta = 0^\circ$ and θ at R.....	26
Figure 3.5: The Parameters used in estimation of the phase center position.....	27
Figure 3.6: Phase of electrical field at $\theta = 0^\circ$ and $\theta = 60^\circ$ for $W_A = 17.78\text{mm}$	29
Figure 3.7: The phase errors versus the radial distance for $W_A = 17.78\text{mm}$	29
Figure 3.8: The phase errors versus the broadside angle for $W_A = 17.78\text{mm}$ aperture...	30
Figure 3.9: The phase errors versus the radial distance R for $W_A = 29.19\text{mm}$	31
Figure 3.10: The phase errors versus the radial distance for $W_A = 43.785\text{mm}$	31
Figure 3.11: The phase errors versus the broadside angle for $W_A = 29.19\text{mm}$	32
Figure 3.12: The phase errors versus the broadside angle for $W_A = 43.785\text{mm}$	33
Figure 3.13: The Parameters used in estimation of the phase center position for taper	34
Figure 3.14: The phase errors versus the broadside angle for $W_A = 17.78\text{mm}$ aperture.....	35

Figure 3.15: The phase errors versus the broadside angle the $W_A = 29.19\text{mm}$ aperture.	35
Figure 3.16: The phase errors versus the broadside angle for $W_A = 43.785\text{mm}$ aperture	36
Figure 3.17: The phase errors versus the radial distance for $W_A = 17.78\text{mm}$	37
Figure 3.18: The phase errors versus the radial distance for $W_A = 29.19\text{mm}$	37
Figure 3.19: Figure 3.18: The phase errors versus the radial distance for $W_A = 43.785$ mm.....	38
Figure 3.20: The phase errors of $W_A = 29.19$ mm multistep for the two phase centers at 2GHz, 2.45GHz and 3GHz.....	39
Figure 3.21: The phase errors of $W_A = 29.19$ mm multistep linear taper for the two phase centers at 2GHz, 2.45GHz and 3GHz.....	40
Figure 3.22: The phase errors of $W_A = 43.785$ mm multi-section transition for the two phase centers at 2GHz, 2.45GHz and 3GHz.....	40
Figure 3.23: The phase errors of $W_A = 43.785$ mm linear taper for the two phase centers at 2GHz, 2.45GHz and 3GHz.....	41
Figure 3.24: The phase errors of $W_A = 43.785$ mm for linear taper and multi-section transitions at the estimated phase center position for 2.45GHz	42

LIST OF SYMBOLS AND ABBREVIATIONS

RLD	Rotman Lens Design
SWP	Standing Wave Pattern
PML	Perfectly matched layer
λ	Wavelength
λ_g	Wave guide length
ϵ_r	Relative permittivity
ϵ_e	Effective relative permittivity
Γ	Reflection coefficient
Z_0	Characteristic impedance
Z_L	Load impedance

Chapter 1

INTRODUCTION

1.1 Introduction

Arrays of radiator elements radiating into a parallel plate region are widely used in microwave and millimeter wave frequencies, as the beam forming networks for multiple beam arrays in communications and other fields [1], [2]. The transmission lines leading into the parallel plate region can be waveguide, coaxial monopoles cables, or microstrip lines. It is necessary to use radiators to launch the electromagnetic waves delivered by these transmission lines into the parallel plate region.

Some of low power applications are constructed on microstrip or stripline configuration as they are cheaper and easier to manufacture [3], [4]. The Rotman lens is one of low power applications that have multi-beam antennas that produce minimally distorted beams within an angular sector of space [1]. This lens operates by equality of path lengths for rays traveling from the source at three perfect focal points to the transmitted phase front, Figure 1.1.

Radiators used between the microstrip lines and the parallel plate regions are commonly linearly tapered type transitions. The linear taper ports of the lens must be placed accurately in the lens in order to reduce phase errors, which is possible only if the phase center position of the ports are well known.

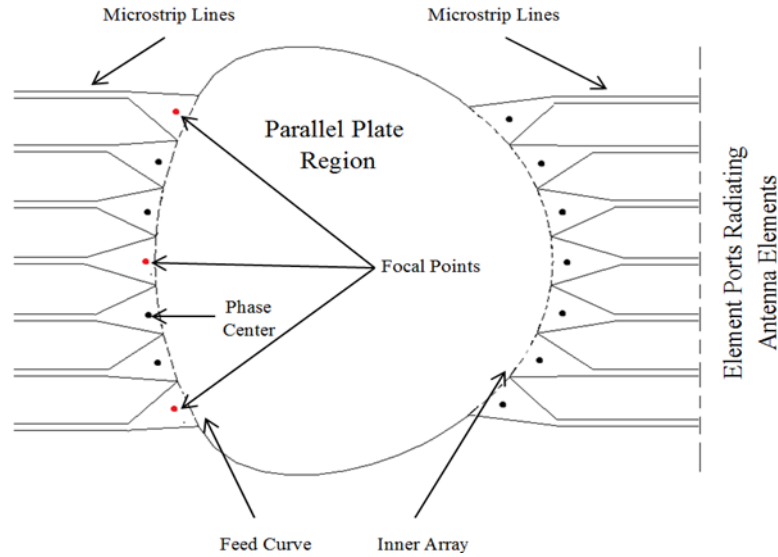


Figure 1.1: Rotman lens geometric design

A parallel-plate region with plate separation less than half a wavelength has been considered by Fong and Smith [5], [6] instead of using entire Rotman lens. The two-dimensional free space has no variation with height in the cavity so Fong and Smith have analyzed the near field in order to obtain the power transmitted between two microstrip horns. In this study two different types of radiators are used to match the 50Ω microstrip line to the parallel plate region. Also the characteristic impedance of the transition between the 50Ω feed line and the wider radiating aperture was evaluated by using the principle of designing multi-section transition into two dimensional parallel plate method [7] by full wave simulation software. The results were compared with the tapered radiator having the same lengths. All design steps are illustrated in Chapter 2.

Three designs of multi-sections transition are used to introduce a simple method for determining the phase center of two dimensional radiators. This method involves the determination of the phase errors against the angle at the far field of the radiator with

reference to the center of the aperture of the radiator. The phase center is then estimated by equating the phases at the broadside and at a chosen angle.

Determination of the phase center of the radiators is very important in Rotman lens fed multiple beam array applications, as the design of these lenses depend on path length equality. Any error in the location of the phase center will cause phase errors and beam deterioration. Although different radiators have been used between the microstrip lines and the parallel plate regions [8], the most commonly used radiators are linearly tapered type transitions [9]. This study the phase center method is applied on multi-section transitions and linear taper radiator .The results of this study show that there is a significant shift from the radiator aperture in the position of the phase center for both types of radiators. The study also shows that the shift in the phase center varies with frequency and distance from the radiator as well as with the physical dimensions of the radiator.

1.2 Thesis Objectives

One of the objectives of this thesis is illustrated the steps to apply the multi-sections technique design to match between the impedance of microstrip feeding line and the impedance of parallel plate aperture for certain widths at design frequency by using full wave simulation software . All the widths of multi-section transitions are designed at 2.45GHz and used to study the phase center positions.

The main objective is introduced and discussed the method that is used to obtain a phase center position of three multi-steps transition that have certain apertures width feeding parallel plate at certain frequency. The results of the phase center are presented according to their widths and after that the same procedure are used to estimate the phase center to three linear tapers have the same width of the multi-

section transitions.

1.3 Thesis Contribution

A matching method was applied between the parallel plate region and 50Ω microstrip lines that fed the parallel plate guide consider a practical problem to decrease the energy loss of the source .A simple method of estimate the phase center for the radiators was successfully applied on different apertures width at design frequency .The result were done by using full wave simulation software.

1.4 Thesis Organization

A matching method was applied to match a 50Ω line to the parallel plate region with low impedance. The calculations of the design parameters for different aperture widths $W_A = \frac{\lambda}{2}, \frac{3\lambda}{4}$ and $\frac{\lambda}{3}$ carried out by using standing wave pattern to build multi-sections taper between the source and the load by using full wave simulation software are covered in Chapter 2. A new phase center position estimation method depending on the phase errors is discussed and tested on three different apertures $W_A = \frac{\lambda}{2}, \frac{3\lambda}{4}$ and $\frac{\lambda}{3}$ in Chapter 3.

Chapter 2

MATCHING TECHNIQUES

2.1 Matching Overview

Matching impedance of transmission line between the source and the load, which is often an important part of a larger design process for microwave system because, imperfect matching increases reflection. Also, the power losses and the phase performance are related with mismatching. The basic idea of general matching is illustrated in Figure 2.1[10].

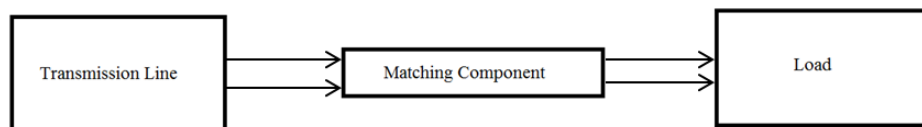


Figure 2.1: Matching circuit diagram

This chapter covers the multi sections transition to match printed Rotman lens as a large parallel plate region with transmission line impedance of 50Ω at the design frequency. It is known that, the impedance of a large parallel plate is very small compared to the impedance of transmission line. In this case, the best procedure to reduce the return loss and attain a gradual energy transformation between the parallel plate region (lens) and transmission line can be achieved by using matching techniques. In following, the models of taper and the multi-sections transition matching techniques will be explained, after giving the details of the Rotman lens.

2.2 Rotman Lens Overview

The first simple design for Rotman lens antenna was done by Rotman and Turner [1], in 1963. Figure 2.2, represents a typical design configuration of the lens where the feeding contour is considered as circular or elliptical, known arc [11].

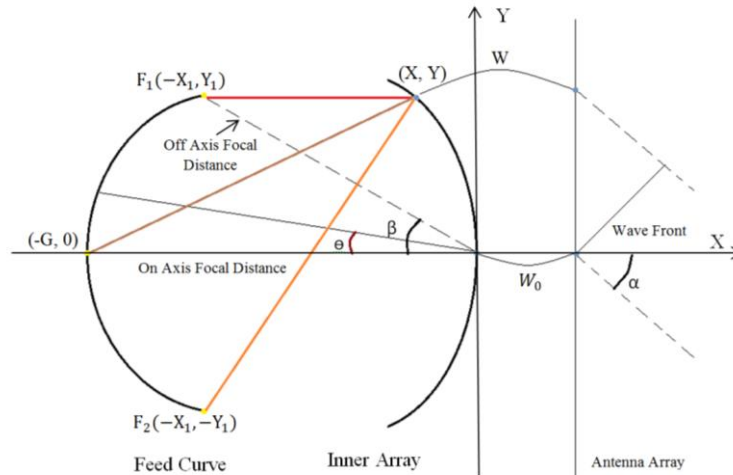


Figure 2.2: Trifocal lens design scheme

The lens is a passive device used as the beam-forming network. It is built by using microstrip techniques, feeding an array antenna to provide large scan angles, high gain, conformal geometry, and low cost. These types of antenna lenses are able to change the direction of the beam, without physically moving the antenna system.

There are a lot of studies and researches in optimizing various parameters which are useful in designing Rotman lens. Descriptions of the Rotman lens parameters are summarized in Table 2.1.

Table 2.1: Rotman Lens Parameters

F	Off-axis focal length
F_1, F_2	Symmetrical Off-axis focal points
G	On-axis focal length
N	Number of array elements
W	Length of transmission line
X_1, Y_1	Coordinate of the typical beam port phase centers.
X, Y	Coordinate of receiver port phase centers.
A	Scan angle
B	Off center focal angle.

The following mathematical equations obtained by geometrical optics principles were used to design the original lens.

$$F_1P + W + N \sin \alpha = F + W_0 \quad (2.1)$$

$$F_2P + W - N \sin \alpha = F + W_0 \quad (2.2)$$

$$F_0P + W = G + W_0 \quad (2.3)$$

These three equations are used to calculate X , Y and W by equating the path length from each three focal points on the parabolic focal arc to the related phase front [1].

2.3 Linearly Tapered Transition

Figure 2.3, shows an example of the microstrip Rotman lens design. This lens is designed by using RLD software and RLD file was imported to full wave simulation software.

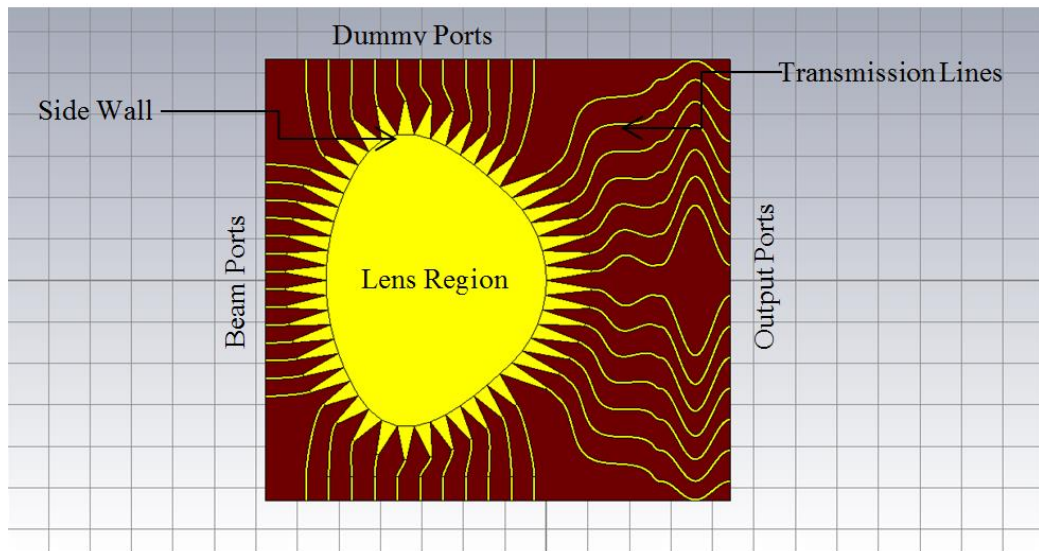


Figure 2.3: Microstrip Rotman lens design

Figure 2.3 shows the arrangement of the input and output ports along the parabolic focal arc and array contour respectively. Also there are loads used to provide reflection less termination of parallel plate region. The field signals are applied to the input ports and are picked up by the output ports. In this case, the field is radiated by a flared microstrip line (linear taper model) into the lens geometry.

The linear taper model is the simplest model that can be used with microstrip Rotman lens. It is used for transition between the 50Ω line and the parallel plate region of the Rotman lens.

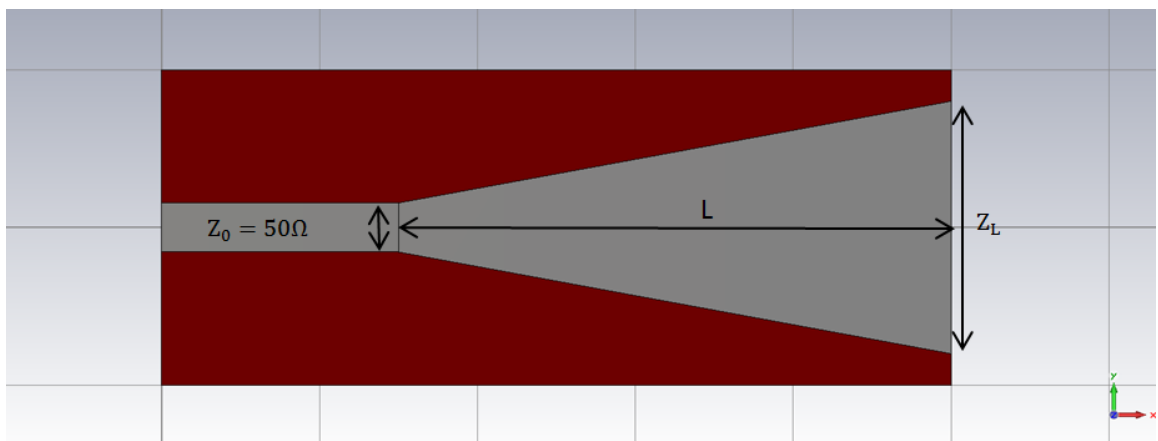


Figure 2.4: Full wave simulation software model of linear taper transition

Equation (2.4) is the basic explanation for obtaining the relationship between the parameters of the linear tapering design, characteristic impedance of the microstrip transmission line Z_0 , the taper length L and the load impedance Z_L [10].

$$Z(z) = Z_0z + s \quad 0 < z < L, s \neq 0 \quad (2.4)$$

Equation (2.4) is the relationship of the model parameters and this relationship is shown in Figure 2.5.

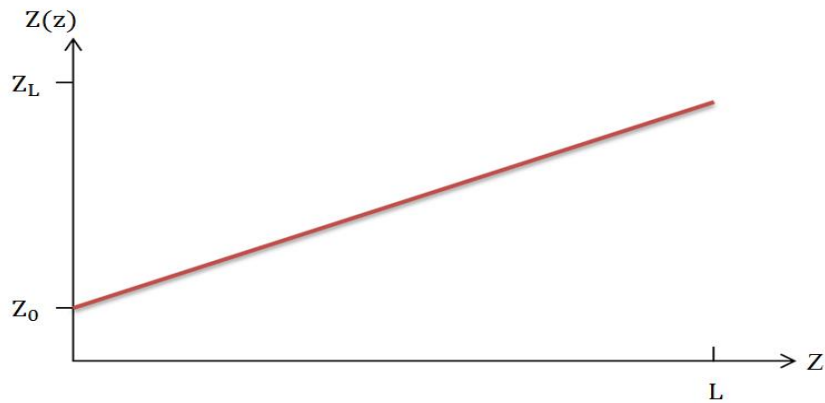


Figure 2.5: Parameter relationship for the linear taper design

2.4 Stepped Transition Model

2.4.1 Rotman Lens as a Parallel Plate Region

In this section, the two dimensional lens antennas is considered as a large parallel plate cavity with apertures between the microstrip transmission lines and the parallel plate region as illustrated in Figure 2.5. The parallel plate region and the aperture are designed and simulated by using full wave simulation software. The three edges of the parallel plate are terminated by using Perfectly Matched Layer (PML) boundary condition to decrease the reflections from edges. Via a microstrip line the parallel plate is launched by a signal at design frequency. The aim is to match the 50Ω microstrip line to the parallel plate region of the Rotman lens. This study is carried

out by making use of the standing wave pattern of the electric field intensity below the microstrip line in the substrate [7]. The information of SWP, gives an idea about the capacitive reactance of the load. Uyguroğlu and Öztoprak calculated the length of the line corresponding to the capacitive reactance and by subtracting this value from the section lengths; they achieved a good matching between the microstrip line and the parallel plate region.

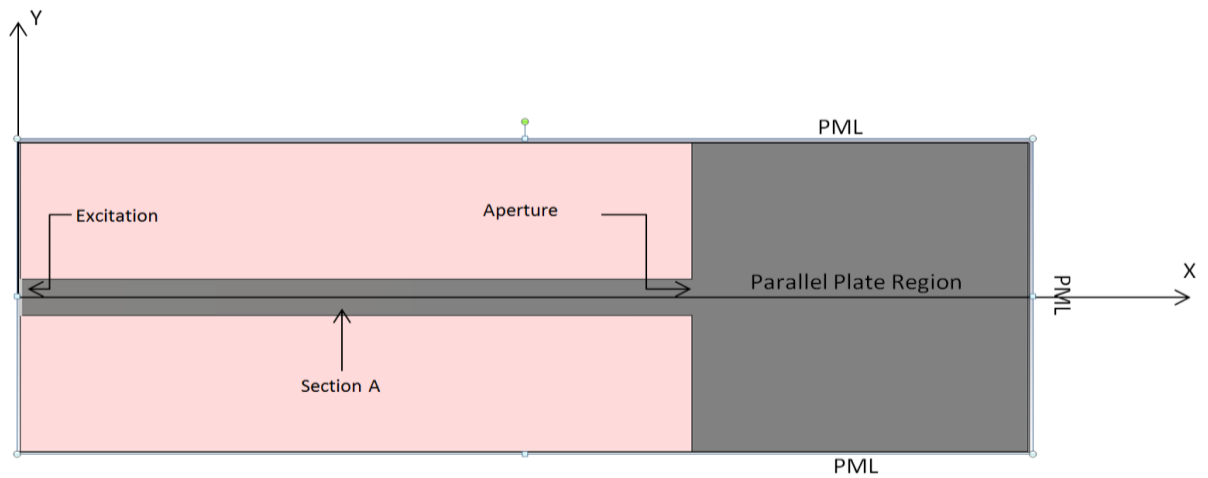


Figure 2.6: Parallel plate region connected with microstrip line

2.4.2 Standing Wave Pattern

The standing wave pattern shown in Figure 2.7 is the magnitude of the normal component of the electric field under the microstrip line.

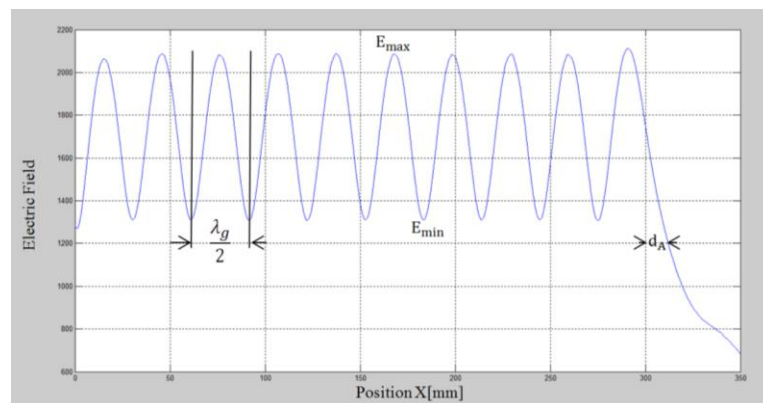


Figure 2.7: Standing wave pattern curve

From the curve of the standing wave pattern shown in Figure 2.7 the shift of the minimum of the field from the aperture position is defined as d_A . This shift is caused by the reactance at the discontinuity between the parallel plate region and the aperture [7], [11]. It is easy to calculate this shift from the aperture by using $(\frac{\lambda_g}{2} - d_A)$, where λ_g is the wavelength of the microstrip line at the frequency of design and was estimated by using by estimate the normal component of the field intensity within the substrate between the conductors along X-axis in the middle of the microstrip line and the parallel plate (SWP).

By using the information that is obtained from Figure 2.7, the radiation impedance of the parallel plate Z_R , the length of section A can be calculated, the reflection coefficient and standing wave ratio S by using following formulas [7]:

$$L_A = \frac{\lambda_g}{4} - d_A \quad (2.4.1)$$

$$Z_R = Z_A \times \frac{1 - |\Gamma|}{1 + |\Gamma|} \quad (2.4.2)$$

The design parameters of the microstrip line in Figure 2.8 are the width of the strip line (W), the thickness of the strip (t), the height of the substrate (h) and the permittivity of the substrate ϵ_r .

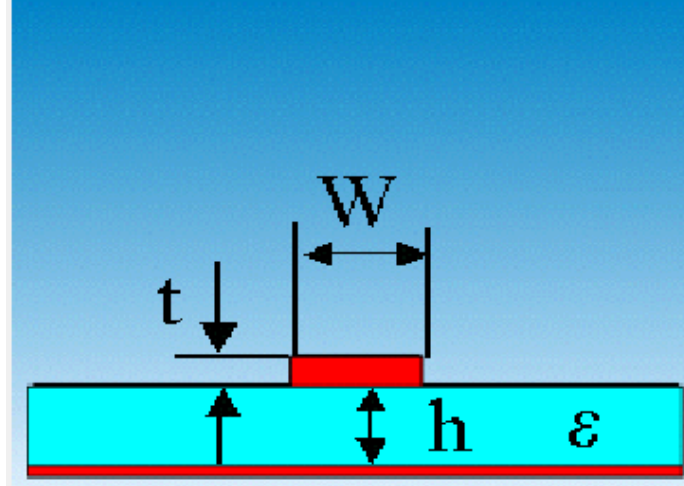


Figure 2.8: Microstrip line parameters

By using these parameters Z_A and effective permittivity ϵ_e can be calculated by using the following equations:

When $\left(\frac{W}{h}\right) < 1$

$$\epsilon_e = \frac{\epsilon_r + 1}{2} + \frac{\epsilon_r - 1}{2} \left[\left(1 + 12 \left(\frac{h}{W} \right) \right)^{-\frac{1}{2}} + 0.04 \left(1 - \left(\frac{W}{h} \right) \right)^2 \right] \quad (2.4.3)$$

$$Z_0 = \frac{60}{\sqrt{\epsilon_e}} \ln \left(8 \frac{h}{W} + 0.25 \frac{W}{h} \right) \Omega \quad (2.4.4)$$

When $\left(\frac{W}{h}\right) > 1$

$$\epsilon_e = \frac{\epsilon_r + 1}{2} + \frac{\epsilon_r - 1}{2} \left[\left(1 + 12 \left(\frac{h}{W} \right) \right)^{-\frac{1}{2}} \right] \quad (2.4.5)$$

$$Z_0 = \frac{120\pi}{\sqrt{\epsilon_e} \left[\frac{W}{h} + 1.393 + \frac{2}{3} \ln \left(\frac{W}{h} + 1.444 \right) \right]} \Omega \quad (2.4.6)$$

After determining Z_A , the radiation impedance Z_R can be calculated.

$$Z_R = Z_A \left(\frac{1-|\Gamma|}{1+|\Gamma|} \right) \quad (2.4.7)$$

And $|\Gamma|$ and S can be calculated from the Figure 2.7 as it is mentioned before.

$$|S| = \frac{E_{max}}{E_{min}} \quad (2.4.8)$$

$$|\Gamma| = \frac{S - 1}{S + 1} \quad (2.4.9)$$

$|\Gamma|$ is always smaller than or equal to one.

2.4.3 Multi-Section Transition

Quarter wave transformer is applied by many different design techniques [8] to match a load to 50Ω transmission line. Figure 2.9 shows the multi-section transition design explained in [7].

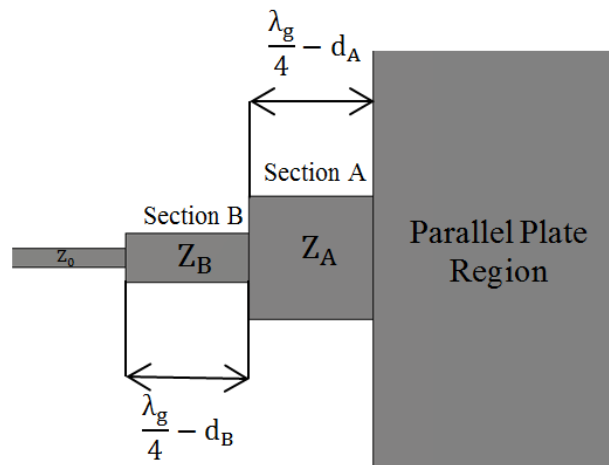


Figure 2.9: Three multi-sections transition

The ordinary microstrip line usually has $Z_0 = 50\Omega$. The matching between microstrip line and the impedance of section A as mentioned before depends on W_A and L_A . The length of section A is obtained by the Equation (2.4.1), while the width of section A (aperture width) is considered as a given parameter, both of section A and B are assumed to be quarter wave length.

2.5 The Simulation Results of the Multi-sections Design

In this part of the study, a multi-sections technique [7] is applied on different aperture width at frequency 2.45GHz. Full wave simulation software is used for the evaluation of the reflection coefficient S11. The reflection coefficient results for the multi-sections and linear taper transitions having same aperture widths and same lengths were compared. The wavelength at the design frequency 2.45GHz is 58.38mm. This wavelength is used to calculate the lengths of section A for three different aperture widths $W_A = \frac{\lambda}{2}, \frac{3\lambda}{4}$ and $\frac{\lambda}{3}$. First design was for section A with 17.78mm as shown in Figure 2.10.

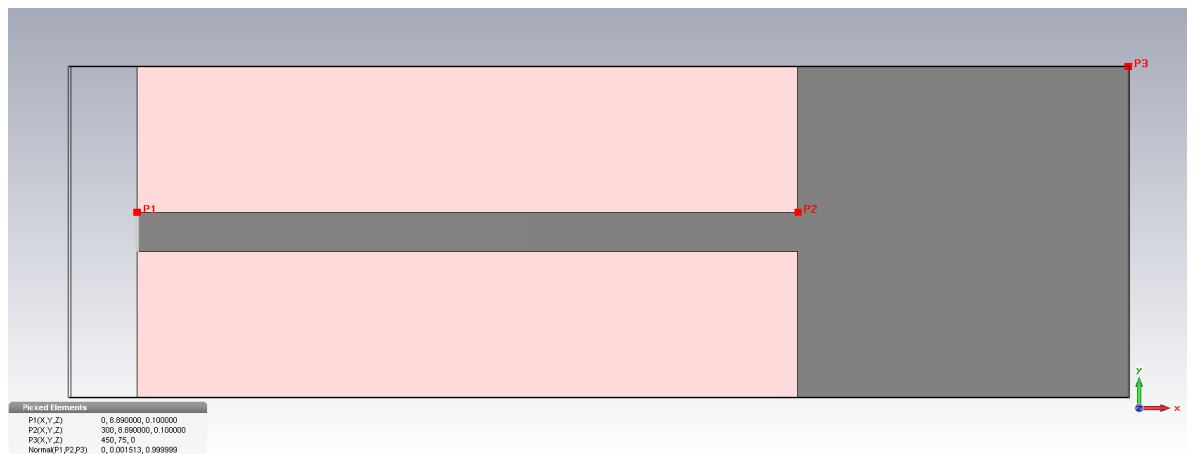


Figure 2.10: 17.78mm aperture width with a microstrip feeding line

All the parameters details and substrate specifications are listed in Table 2.2

Table 2.2: Design parameters of the parallel plate structure

Design Frequency	Substrate Permittivity	Conductor Thickness	Substrate Thickness	Aperture Width	Parallel Plate Dimensions
2.45GHz	4.4	0.1mm	1.6mm	17.78mm	300 × 300mm ²

SWP illustrated in Figure 2.11 was obtained as explained in section 2.4.2.

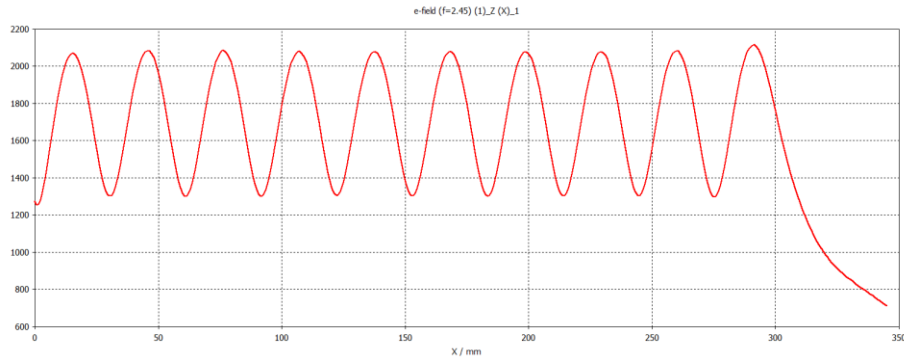


Figure 2.11: Standing Wave Pattern of $W_A = 17.78\text{mm}$ Aperture

The SWP in the Figure 2.11 shows that $\lambda_g = 30.59\text{mm}$ and $d_A = 5.74\text{mm}$. By using Equation 2.4.1 the length of the section A was calculated to be $L_A = 9.54\text{mm}$. The maximum and minimum values of the electric field intensity are estimated from Figure 2.11, as 2081.8 V/m and 1298 V/m respectively. Using these values $S = 1.6$ and $|\Gamma| = 0.23$.

Considering that, the width of the section A is 17.78 mm, $\epsilon_r = 4.4$ and $h = 1.6$ mm. Z_A is calculated by using the Equations 2.4.6 to be 13.49Ω . The impedance of section B is calculated by using the impedance of the parallel plate $Z_R = 8.4 \Omega$ and the input impedance of the quarter wave length section $Z'_R = \frac{Z_A^2}{Z_R} = 21.7 \Omega$. $Z_B = \sqrt{Z_0 \times Z'_R}$ which is 32.84Ω .

From the Z_B , the width of section B is determined by using the transmission line theory and apply Equations 2.4.6. The value is evaluated to be 5.8 mm.

The length of the section B was estimated in the same way.

Define:

$$L_B = \frac{\lambda_g}{4} - d_B \quad (2.4.10)$$

The SWP under the section A and B was evaluated by removing the parallel plate region from the previous structure. As it shown by Figure 2.12 microstrip line of section A was terminated by PML absorbing boundary condition.

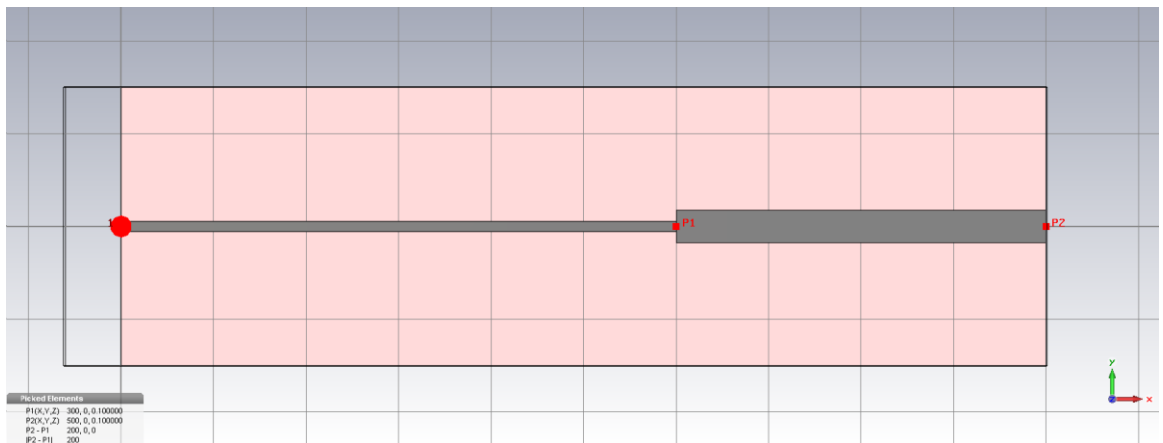


Figure 2.12: Section A and section B

The SWP of structure of Figure 2.12 is given by Figure 2.13. ($\lambda_g = 64.37\text{mm}$ and $d_B = 0.72\text{mm}$) are extracted from Figure 2.13 using Equation 2.4.10. The length of section B was estimated to be 15.38mm.

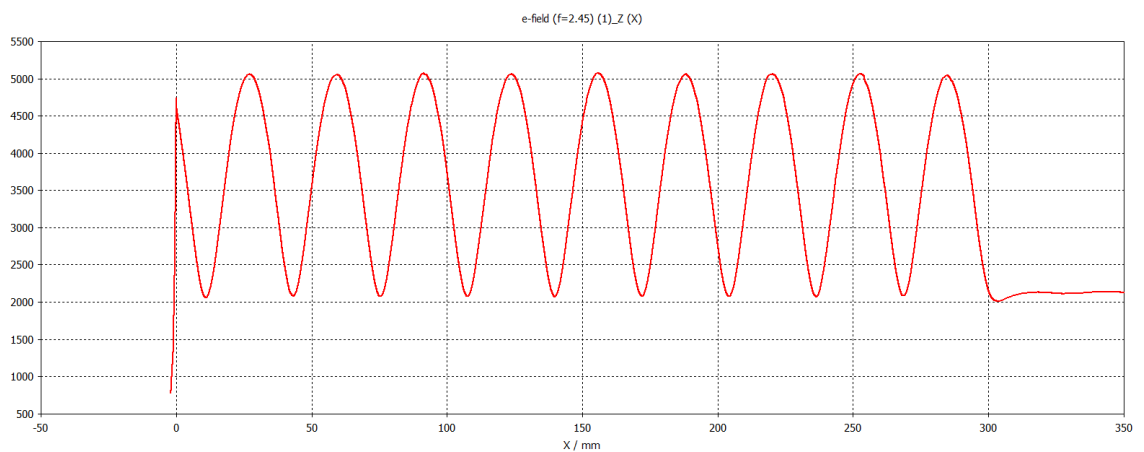


Figure 2.13: Standing wave pattern of section B and section A

After estimating all the dimensions of section A and B the final multi-sections geometry was obtained. Figure 2.14 shows the final multi-sections transition between 50Ω line and the parallel plate region.

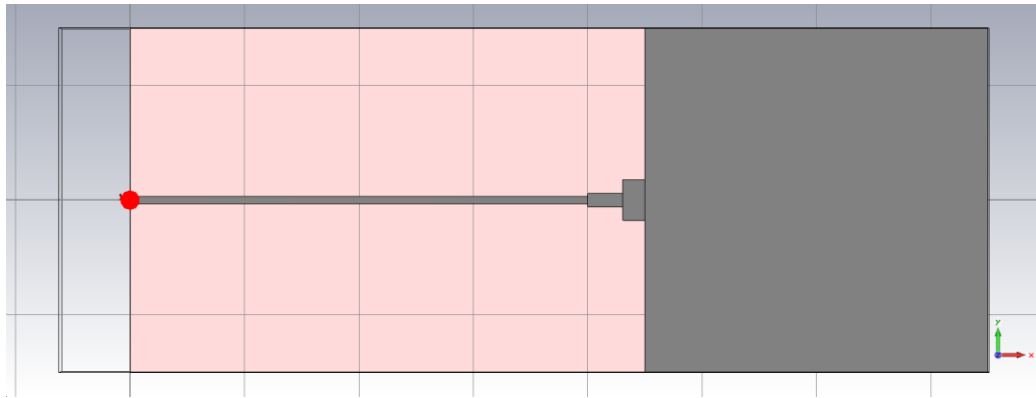


Figure 2.14: Final multi-section design

Figure 2.15 describes the dimensions of $W_A = 17.78\text{mm}$ multi-sections of the transition.

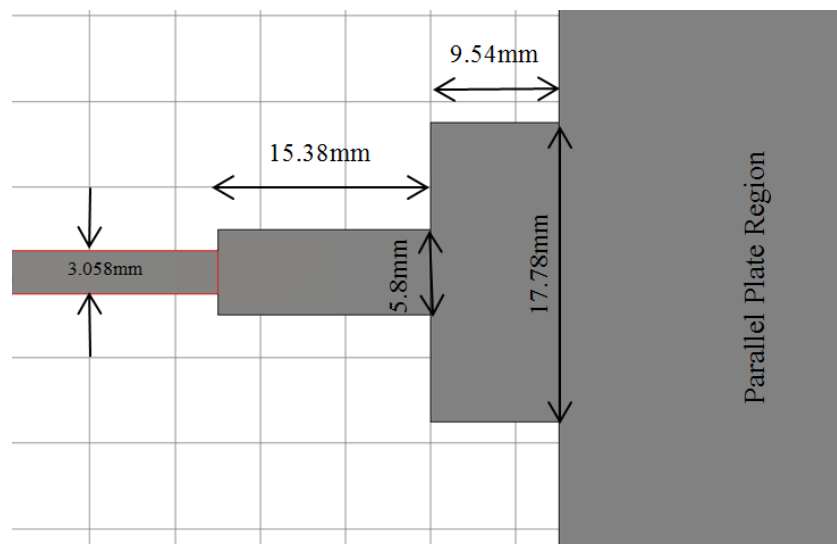


Figure 2.15: Dimension of multi-sections design

The simulation results indicate a very good matching at the design frequency 2.45 GHz. Figure 2.16 shows the return loss of the transition for 1GHz -4GHz band.

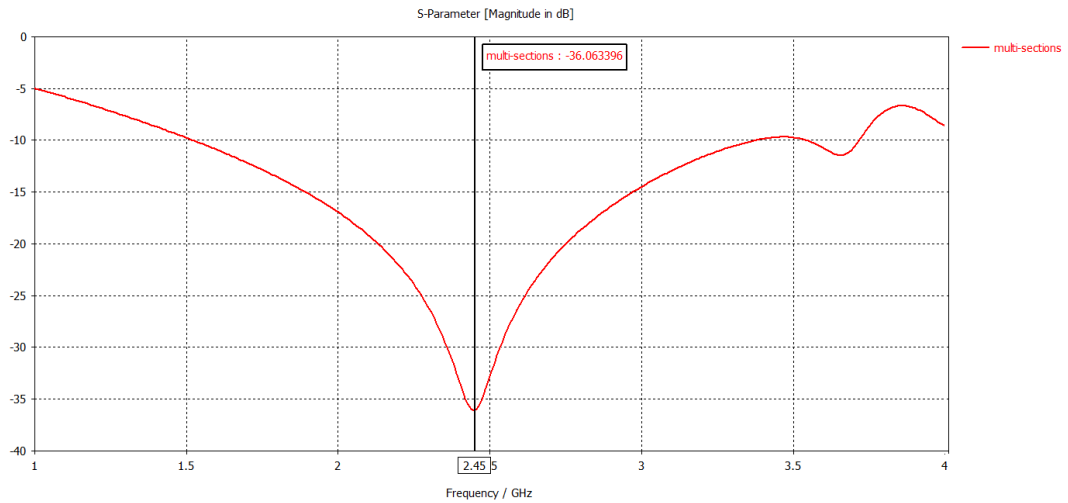


Figure 2.16: The return loss for multi-section transition (17.78mm)

The same aperture width and length was applied on linearly tapered transition and it is simulated by full wave simulation software at the design frequency 2.45GHz to compare the return loss results. The structure of the transition is given by Figure 2.17. Figure 2.18 shows comparison of the return loss of the multi-sections transition and linear tapered transition.

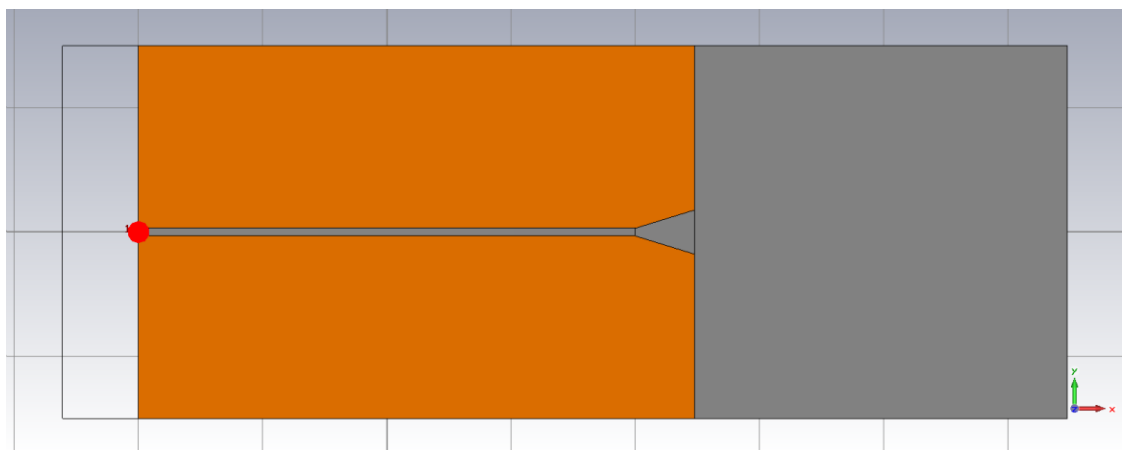


Figure 2.17: linearly tapered transition between 50Ω line and the parallel plate region

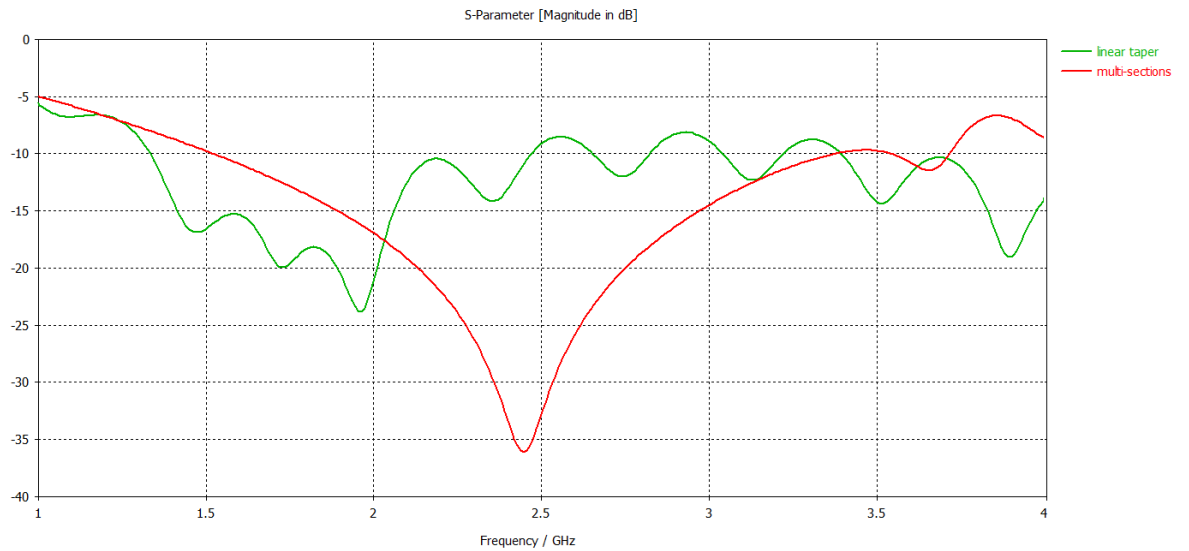


Figure 2.18: Comparison S11 of linearly tapered transition and multi- steps transition

Acceptable matching between the 50Ω transmission line and the parallel plate region was achieved successfully at the design frequency 2.45GHz by using multi-sections transition with reflection coefficient of about -35dB . Similar study has been carried out for different aperture widths $W_A = \frac{\lambda}{3}, \frac{\lambda}{2}$ and $\frac{3\lambda}{4}$. The results are summarized in Table 2.3.

Table 2.3: The values and the dimensions of three multi-section parameter designs.

W_A	17.78mm	29.19mm	43.785mm
d_A	5.74mm	7.19mm	6.2mm
L_A	9.54mm	7.9mm	8.744mm
Z_A	13.49Ω	8.7Ω	5.97Ω
$ S $	1.6	1.315	1.12
$ \Gamma $	0.23	0.136	0.057
Z_R	8.4Ω	6.62Ω	5.33Ω
Z_R'	21.7Ω	11.43Ω	6.69Ω
Z_B	32.84Ω	23.91Ω	18.28Ω

W_B	5.8mm	8.72mm	12.24mm
d_B	0.72mm	1.47mm	3.99mm
L_B	15.38mm	14.3mm	11.557mm

The return loss simulation results for $W_A = \frac{\lambda}{2}$ and $W_A = \frac{3\lambda}{4}$ for multi-section transition designs are compared with the linear tapered design of the same length and same width. The designs are illustrated in Figure 2.19.

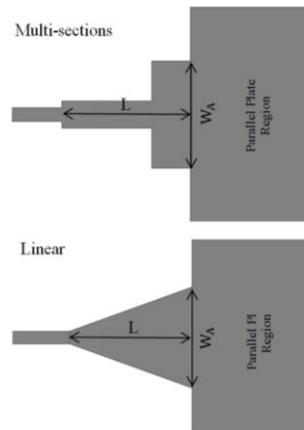


Figure 2.19: Multi-section and linearly tapered designs

The return loss comparison of the $W_A = \frac{\lambda}{2}$ illustrated in Figure 2.20. It is clear from the curves below that the multi-section transition has minimum return loss of about 40dB at 2.45GHz.

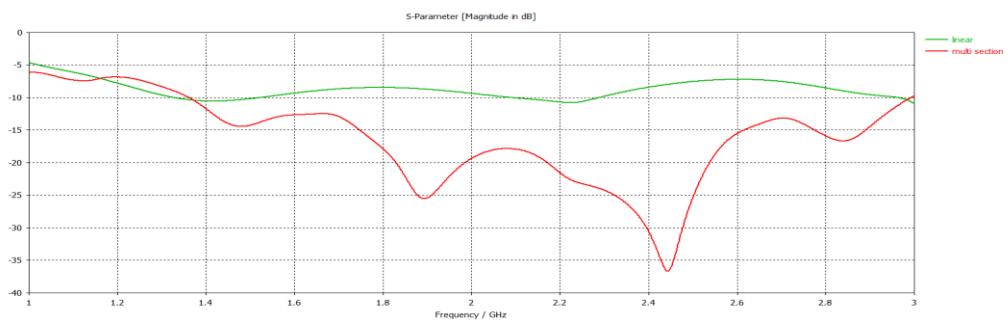


Figure 2.20: Return loss curves for multi-section and linear taper transitions ($W_A = \frac{\lambda}{2}$)

The same strategy is used to obtain the return loss for $W_A = \frac{3\lambda}{4}$ aperture. Figure 2.21 shows the curves of reflection coefficient for both transitions.

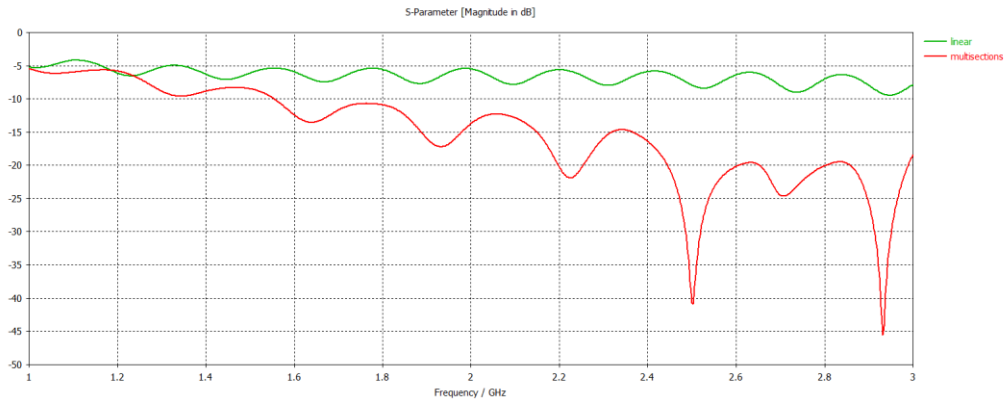


Figure 2.20: Return loss curves for multi-section and linear taper transitions ($W_A = \frac{3\lambda}{4}$)

It is observed from Figure 2.19, 2.20 and 2.21 that it is possible to achieve better matching by using the multistep transition by using shorter transition lengths, which minimizes the dimensions. This kind of transition is suitable for Rotman lens antenna to reduce the antenna dimensions and also achieve lower phase errors.

Chapter 3

THE PHASE CENTER POSITION

3.1 Determination of the Phase Center

3.1.1 Electrical Field Radiated by the Multi-section transition

There are several microwave applications that use arrays of radiating ports into a large parallel plate. Fong and Smith [5], [6] have used two dimensional aperture theory to analyze the field radiated into a parallel plate waveguide with plate separation less than half wavelength. The field does not vary with the height between the conducting plates.

The parallel plate region may be fed by a linearly tapered microstrip or multi-sections transition. There are many number of beamforming networks (PFNs) constructed on configuration of stripline and microstrip line [3], [4].

These transitions may cause problems like phase errors when the aperture widths increase, because these parallel plate transition regions are not radiating from a point. A special care must be taken to find the position of the phase center for these kinds of radiation structures. In this study a simple method is suggested for multi-section and linear taper transitions.

In this chapter, the position of the phase center of number of different widths microstrip multi-section transitions fed parallel conducting plate regions are presented. The method of design and all design parameters of the multi-sections

transitions are illustrated in Chapter 2. Figure 3.1 shows the electric field distribution of the microstrip multi-sections transitions for a radiator of widths $W_A = \frac{\lambda}{3}$ mm radiating into a 300 mm \times 300 mm parallel plate region separated by 1.6 mm. The plate is placed on FR4 substrate.

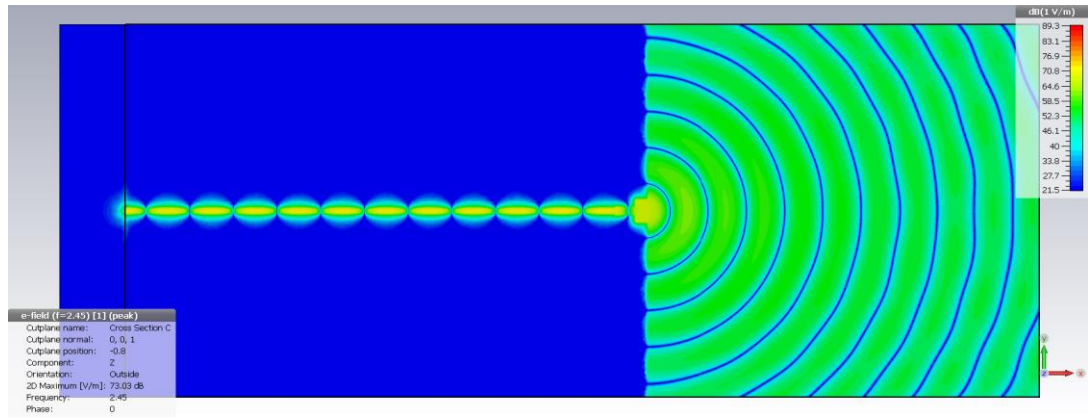


Figure 3.1: The electric field Intensity of multi-section transition below the Parallel Plate region for $W_A = 17.78$ mm.

The electric field intensity of the aperture having $W_A = 17.78$ mm, for multi-section transition below the parallel plate is shown by Figures 3.1. The phase front of the electric field for $W_A = 17.78$ mm aperture width is almost cylindrical, while the phase fronts for the wider apertures become more planar for a particular angular region as in Figure 3.2.

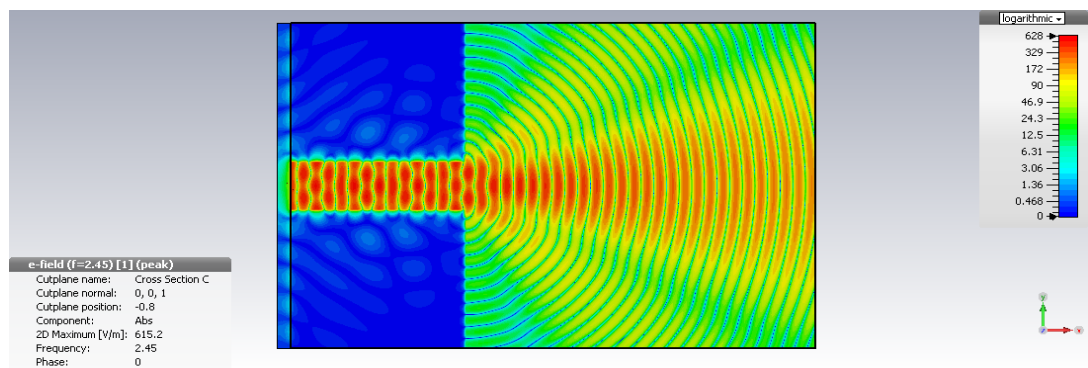


Figure 3.2: The electric field intensity of wide aperture below the parallel plate region for $W_A = 58.38$ mm

The far field pattern below the parallel plate at a distance $R=2.81\lambda$ for $W_A = 17.78\text{mm}$ aperture width is shown in Figure 3.3. The maximum value of the gain for this multi-sections is around 3 dB.

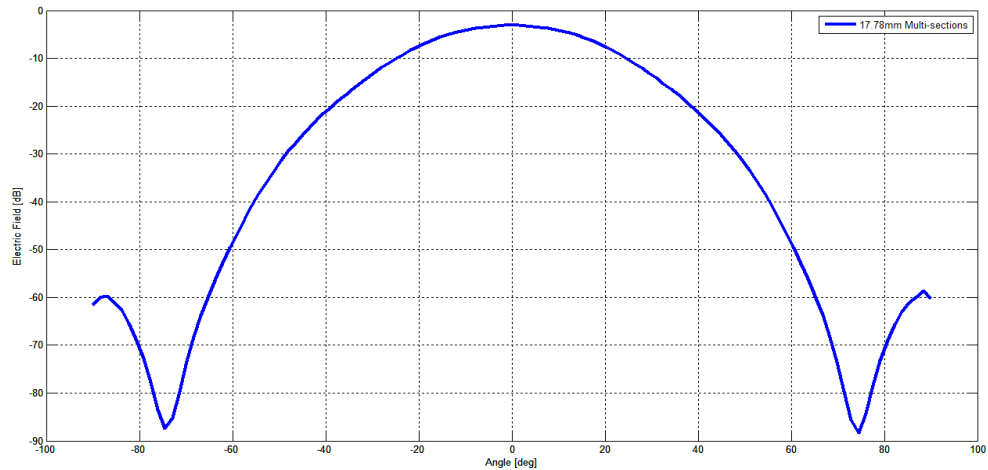


Figure 3.3: Radiation pattern at $R=2.8\lambda$ for $W_A = 17.78$ mm aperture width

3.2 Phase Center Estimation

The electric field lines may have cylindrical equiphasic surfaces for a particular angular region and the axis of the cylinders is called a phase center [1]. The particular equiphasic surface is defined as the curve passing through the point of observation .i.e. R . But when the radiating region is not a point, the phase center position may vary. This variation causes phase errors.

By comparing the phases at two angles, it can show that there is a certain shift between these phases. This shift is shown in Figure 3.4. From this shift it is obvious that the center of the phase is not at the origin of the coordinate system.

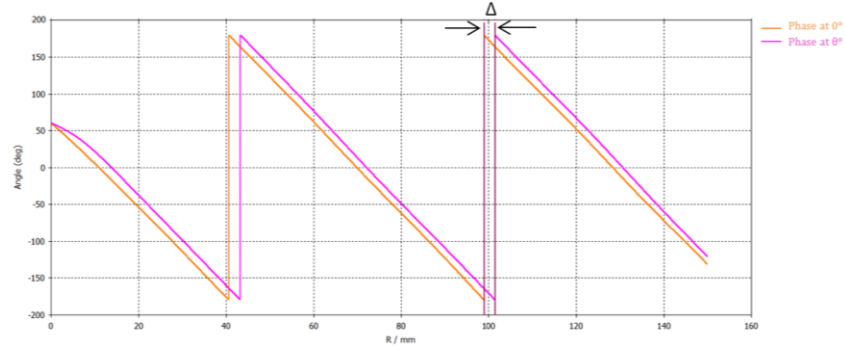


Figure 3.4 : The Phase error between $\theta = 0^\circ$ and θ at R aperture

In this study, a simple method is suggested to estimate the position of the phase center. The study has been carried out by evaluating the phase of the electric field intensity using available full wave simulation software. The zero reference point of the phase was taken to be the center of the aperture. The phase error Δ , at a distance R from the reference point is defined as the difference between the ideal phase front and the computed phase front. The Δ value is used to correct the position of the phase center and reduce the phase errors. Figure 3.4 is used for this purpose.

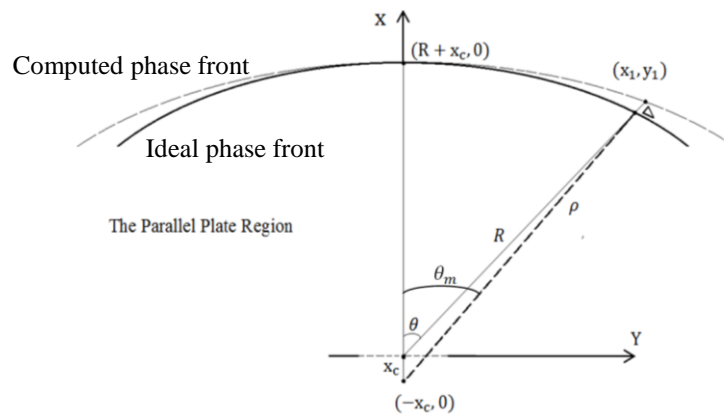


Figure 3.4: The parameters used in estimation of the phase center position

The phase error was estimated by comparing the electric field phase below the parallel plate region at distance R at $\theta = 0^\circ$ and the phase of the electric field at the same distance for another angle. The main idea here to find the phase center position

for the transition that has zero phase error by finding a simple mathematical relationship between the Δ , R , θ_m and the position of the phase center x_c at the far field region as illustrated in Figure 3.4.

The distance from the aperture center to the phase center x_c is calculated by equating the phases at broadside $\theta = 0$ and a chosen angle θ_m . This angle can be the largest angle used from the phase center. By equating the distance x_c+R and ρ can show that:

$$(x_1 - (-x_c))^2 + y_1^2 = (x_c + R)^2 \quad (1.3)$$

Where

$$x_1 = (\Delta + R) \cos \theta$$

$$y_1 = (\Delta + R) \sin \theta$$

The phase center position x_c is obtained by solving equation 3.1 can be shown that:

$$x_c = \frac{\Delta^2 + 2R\Delta}{2R - 2(R + \Delta) \cos(\theta)} \quad (3.2)$$

R is taken to be sufficiently large so that the phase values are obtained in the far field. Equation 3.2 was applied on multi-section transitions and the liner taper and the result of phase error at x_c by using full wave simulation software is attained the main aim of getting zero phase error at the far field in this study.

3.3 The Phase Center Simulation Result

In this section, a method for estimating the position of the phase center is presented here by using the previous simulation phase result to estimate the phase difference of radiating field in two different angular directions.

In order to compare phase error for the multi-sections transition and linear taper, Equation 3.2 was applied to estimate the phase centers. R and θ were taken to be 2.81λ and 60° respectively. The phase error results between the phase in angular directions between 0° and 60° were simulated for the same distance R from the center of radiator aperture for all previous structures having $W_A = \frac{\lambda}{3}, \frac{\lambda}{2}$ and $\frac{3\lambda}{4}$ for multi-section transition and linear taper given in Chapter 2.

3.3.1 Phase Center of The Multi-sections Transitions

The phase error between the phases at two angles $\theta = 0^\circ$ and $\theta = 60^\circ$ from the center of three different aperture widths $W_A = \frac{\lambda}{3}, \frac{\lambda}{2}$ and $\frac{3\lambda}{4}$ to the ideal phase front at distance $R=2.81\lambda$ along the parallel plate region were examined. This shift in the phase was used to calculate the phase center position for the multi-sections designs, as shown by Figure 3.5. The phase error along $R=2.81\lambda$ mm from the aperture center to the ideal front phase for radiator aperture of $W_A = 17.78$ mm between $\theta = 0^\circ$ and $\theta = 60^\circ$ was measured to be 2.38 mm. After substituting 2.38 mm in Equation 3.2 the position of the phase center was calculated to be 4.894 mm.

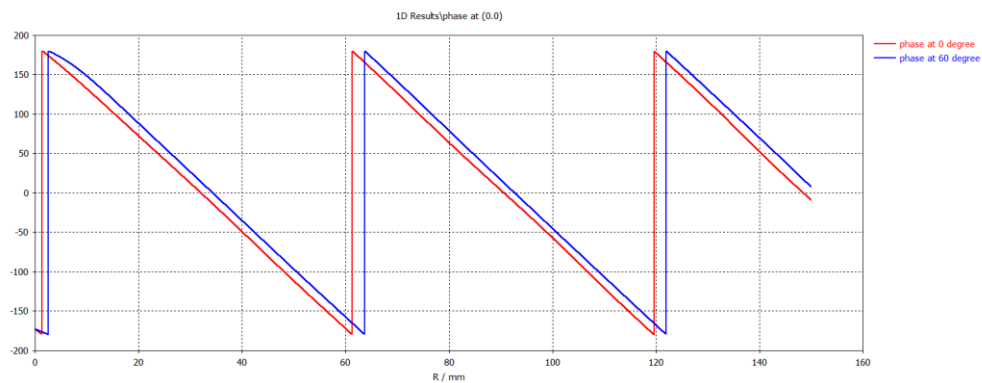


Figure 3.5: Phase of electrical field at $\theta = 0^\circ$ and $\theta = 60^\circ$ for $W_A = 17.78$ mm Aperture

The phase error between two angles $\theta = 0^\circ$ and $\theta = 60^\circ$ along $R + x_c$ from the estimated phase center position to the computed phase front was determined to be

zero at the far field as illustrated by Figure 3.6 and Figure 3.7.

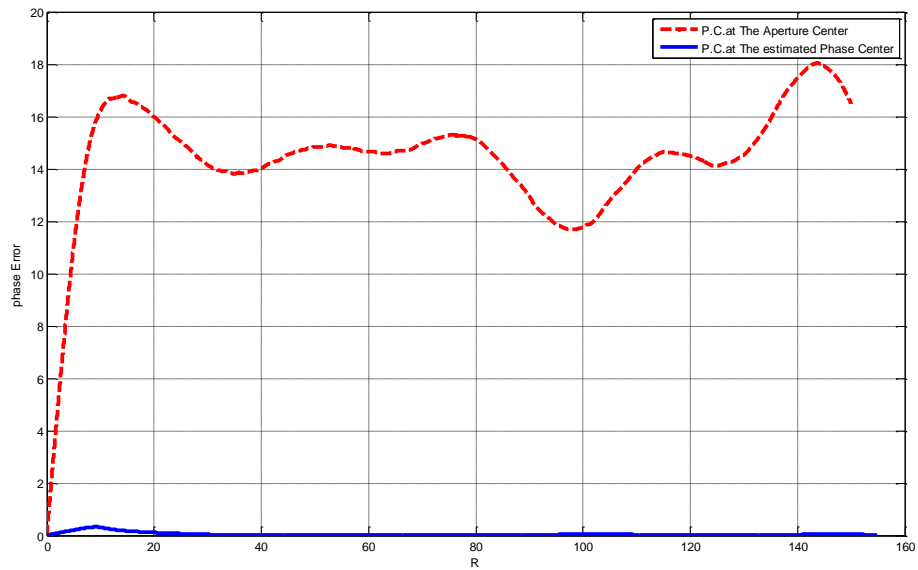


Figure 3.6: The phase errors versus the radial distance for $W_A = 17.78\text{mm}$

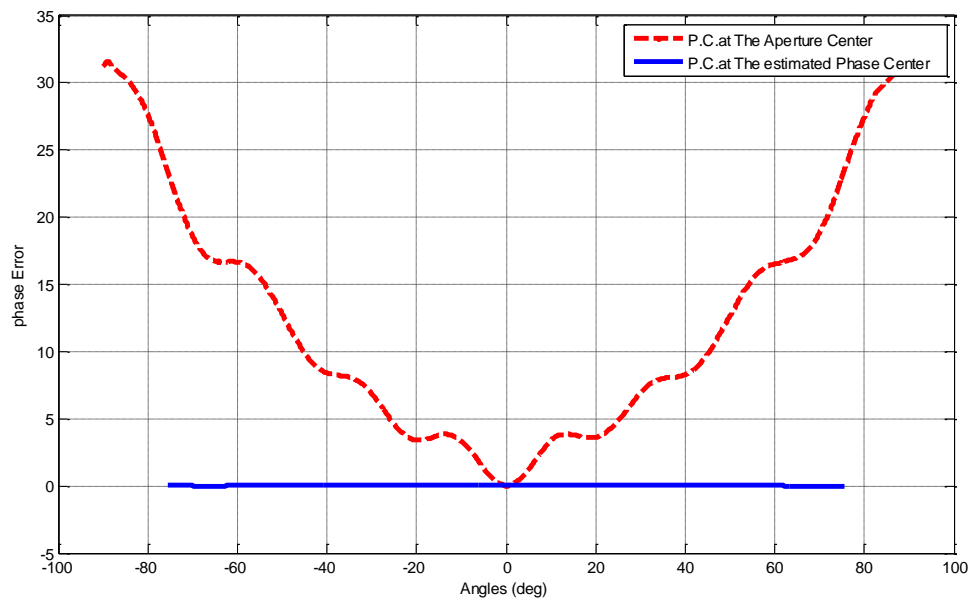


Figure 3.7: The phase errors versus the broadside angle for $W_A = 17.78\text{mm}$ aperture

The same procedure is used to obtain the phase error and the phase center position for

$W_A = \frac{\lambda}{2}$ and $\frac{3\lambda}{4}$ apertures of the multi-section radiator, All the given and the

measurements and calculated values are given by Table 3.1

Table 3.1: The values of parameters of the phase center position of multi-section.

W_A	l	Δ	x_c
29.19mm	22.2mm	3.369mm	6.97mm
43.785mm	20.301mm	5.466mm	10.6mm

Notice that, for wider apertures the distance between the phase center and the point of the aperture increases. The phase error at $R + x_c$ of $W_A = \frac{\lambda}{2}$ and $\frac{3\lambda}{4}$ apertures are shown in Figure 3.8 and Figure 3.9 respectively .

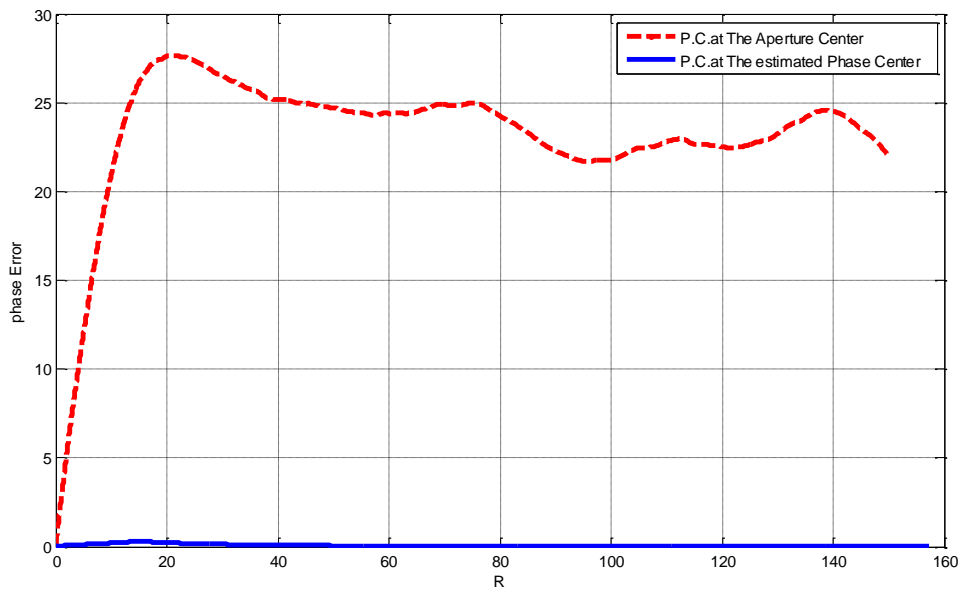


Figure 3.8: The phase errors versus the radial distance R for $W_A = 29.19\text{mm}$

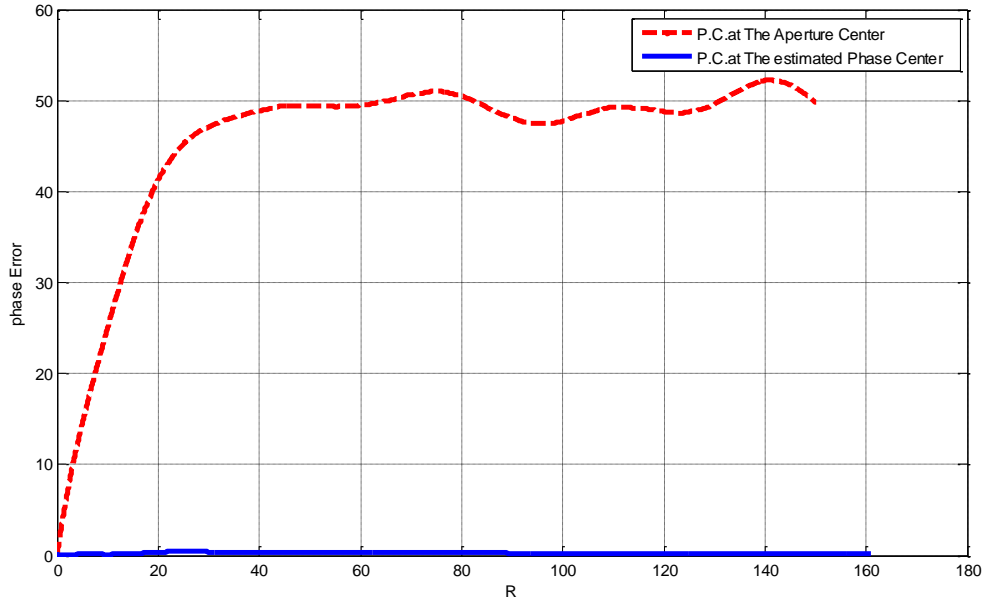


Figure 3.9: The phase errors versus the radial distance for $W_A = 43.785\text{mm}$

Figure 3.8 illustrates the comparison of the phase errors for the phase center at the aperture, and phase center at the estimated point, with respect to the ideal phase front. The figure shows that correction in the phase center results on almost zero phase where it was 20° from the aperture. Figure 3.9 shows the phase difference between two angles for different phase center positions along R and $R + x_c$ for $W_A = \frac{3\lambda}{4}$ aperture width. For instance, at $R=150\text{mm}$ for both of the phase center positions, the phase error was around 50 degree at the center of the aperture and zero degree at the phase center at $x_c = 10.6\text{mm}$.

Figure 3.10 and Figure 3.11 show comparisons of the results of the phase error for both of the estimated phase center and the phase center at the aperture at the ideal phase front and the computed between -90 to 90 degree. The results of phase in Figure 3.10 and Figure 3.11 show a good estimation in the phase center positions since the phase error results are almost zero for $W_A = \frac{\lambda}{2}$ and $W_A = \frac{3\lambda}{4}$.

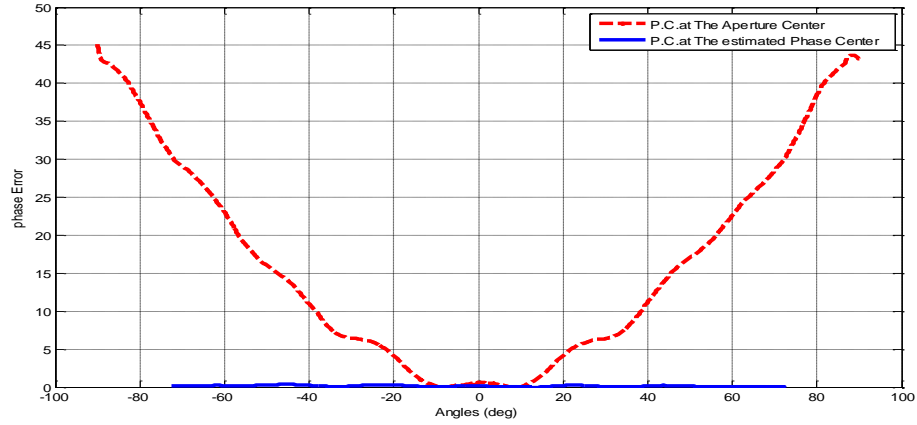


Figure 3.10: The phase errors versus the broadside angle for $W_A = 29.19\text{mm}$

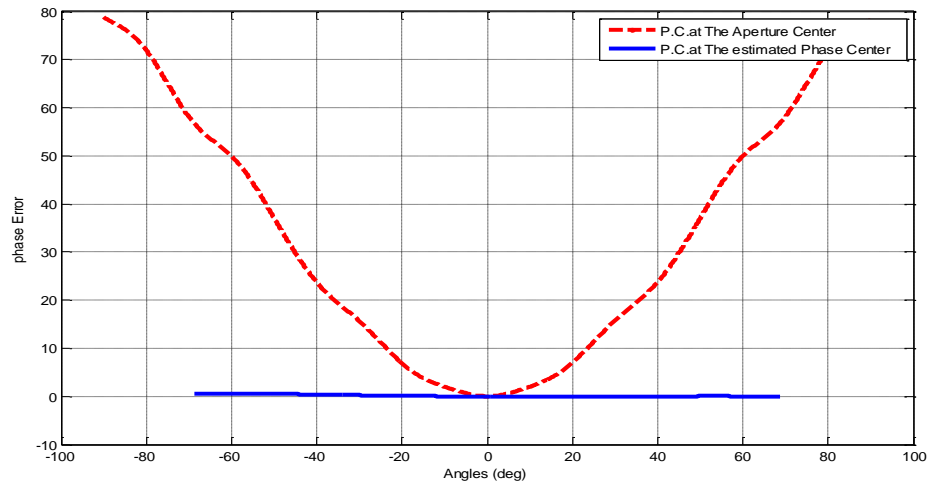


Figure 3.11: The phase errors versus the broadside angle for $W_A = 43.785\text{mm}$

In the following section a similar discussion is carried out for the linear taper transition.

3.3.2 Phase Center of The Linear Taper

In section a linear taper having the length of multisection transition at 2.45GHz is considered. For various aperture widths similar to the previous multi-step design were considered to examine the performance of the phase center estimation method on linear taper transition. The performance is measured in terms of the phase error.

Figure 3.12 shows the geometric parameters of the linear taper that applied in the

previous method .

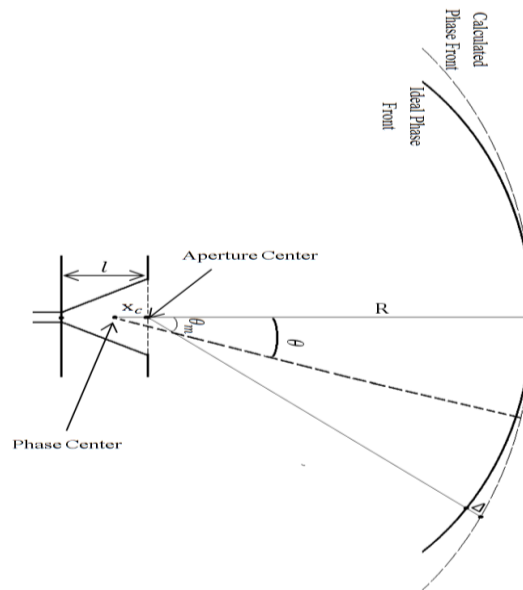


Figure 3.12: The Parameters used in estimation of the phase center position for taper transition

The all values of the geometric parameters for different width linear taper aperture that used to calculate the phase center are listed in Table 3.2 below. The length of the linear taper is the summation of the length of the sections A and B for the multi-section transitions . The phase error of $W_A = \frac{\lambda}{3}, \frac{\lambda}{2}$ and $\frac{3\lambda}{4}$ apertures were obtained from the difference between the phase at $\theta = 60^\circ$ and the phase at the origin of the coordinate system where $\theta = 0^\circ$ along $R=150\text{mm}$ Equation 3.2 was used to calculate the phase center position x_c of the taper.

Table 3.2: The values of parameters of the phase center position of linear taper

W_A	l	Δ	x_c
17.78mm	24.92mm	2.41mm	4.94mm
29.19mm	22.2mm	3.525mm	7.304mm
43.785mm	20.301mm	8.12mm	13.85mm

The result of the phase error for the three tapers is obtained by full wave simulation software with the same procedure that was discussed before with the multi-sections transitions, Figures 3.13, 3.14 and 3.15 show the curves for the phase error at the ideal phase front and the computed phase front at a certain distance.

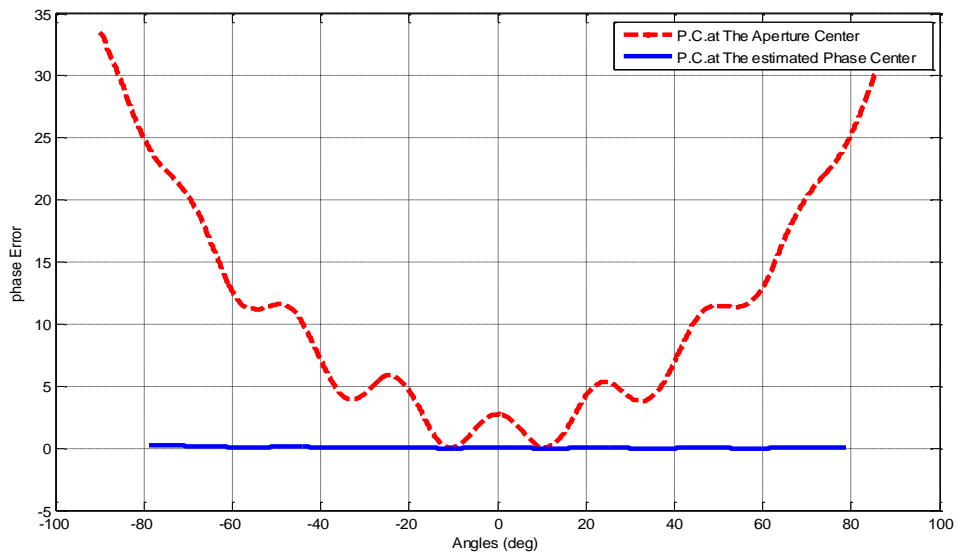


Figure 3.13: The phase errors versus the broadside angle for $W_A = 17.78\text{mm}$ aperture

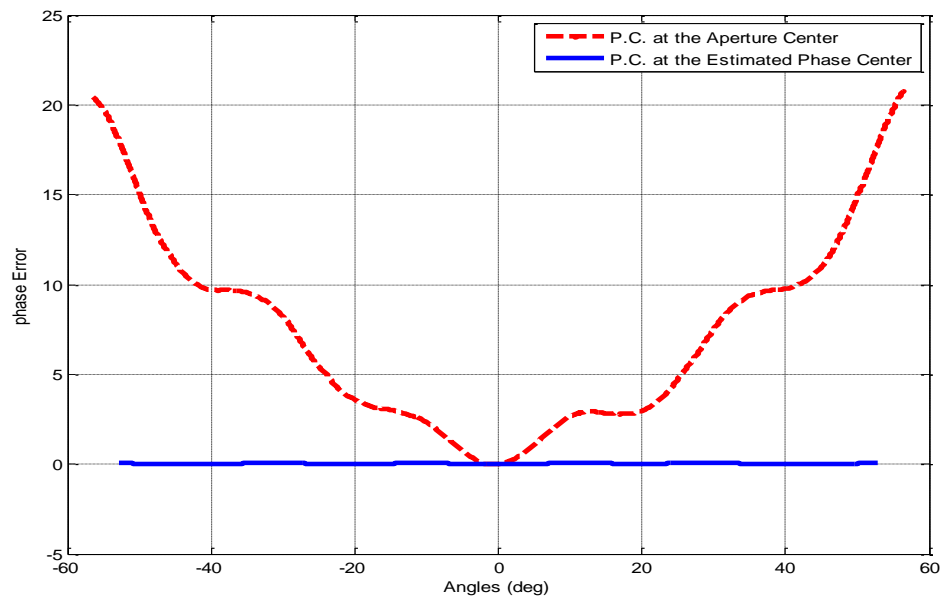


Figure 3.14: The phase errors versus the broadside angle the $W_A = 29.19\text{mm}$ aperture

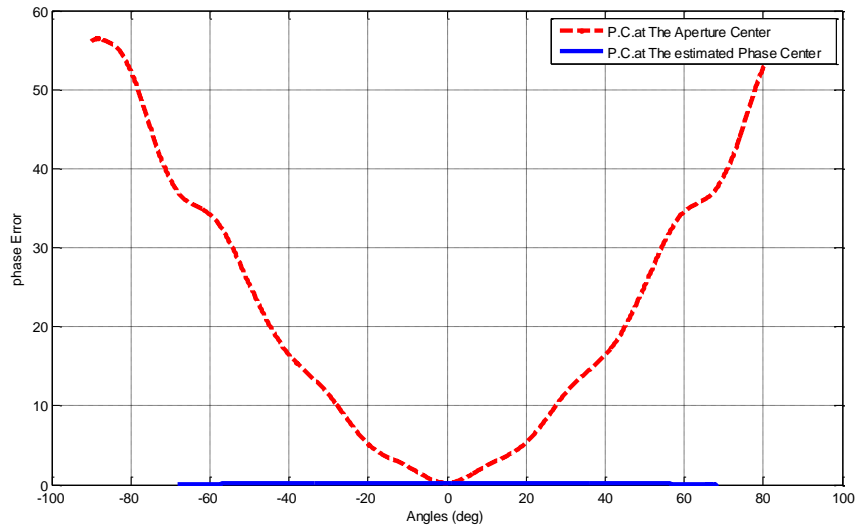


Figure 3.15: The phase errors versus the broadside angle for $W_A = 43.785\text{mm}$

It can be observed from Figure 3.13 the phase deviates significantly from the phase at the broadside with the increasing θ and it is about 12° at $\theta = 60^\circ$. These results clearly indicate that the phase center should be at a distant from the aperture center. By using the Equation 3.2 the phase center was estimated to be $x_c = 2.94\text{mm}$ from the aperture center. The phase center at the estimated center curve show that the phase errors were almost zero between $\theta = 0^\circ$ and $\theta = 60^\circ$ for aperture $W_A = 17.78\text{mm}$. Figure 3.14 shows the phase deviates significantly from the phase at the broadside with the increasing θ and it is more than 15° at $\theta = 60^\circ$ for $W_A = 29.19\text{mm}$ aperture width of the linear taper and the phase center was estimated to be $x_c = 3.525\text{mm}$ from the aperture center by substituted the value of the phase error in Equation 3.2.

For the $W_A = 43.785\text{mm}$ taper the phase center was calculated by the same steps and substituted $\Delta = 8.12\text{mm}$ in the previous formula to be $x_c = 13.852\text{mm}$, this distance is considered as the phase center position for $W_A = 43.785\text{mm}$ linear taper that was designed in Chapter 2. Figure 3.15 illustrates that the phase error at $\theta = 60^\circ$ for

$W_A = 43.785\text{mm}$ aperture was around at $\theta = 35^\circ$ but at the estimated phase center the error was with very low error almost zero as it is clear in Figure 3.16.

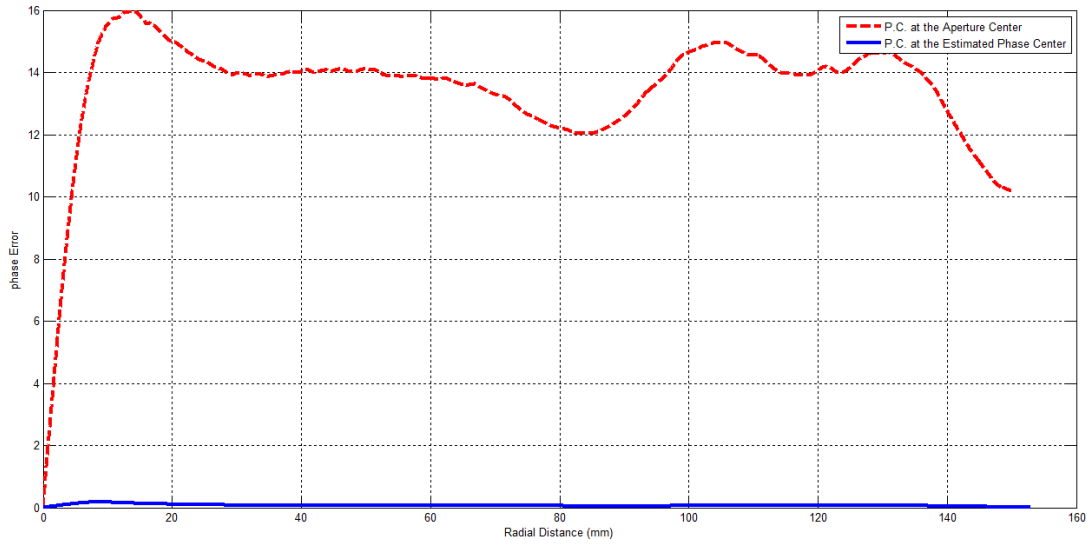


Figure 3.16: The phase errors versus the radial distance for $W_A = 17.78\text{mm}$ aperture

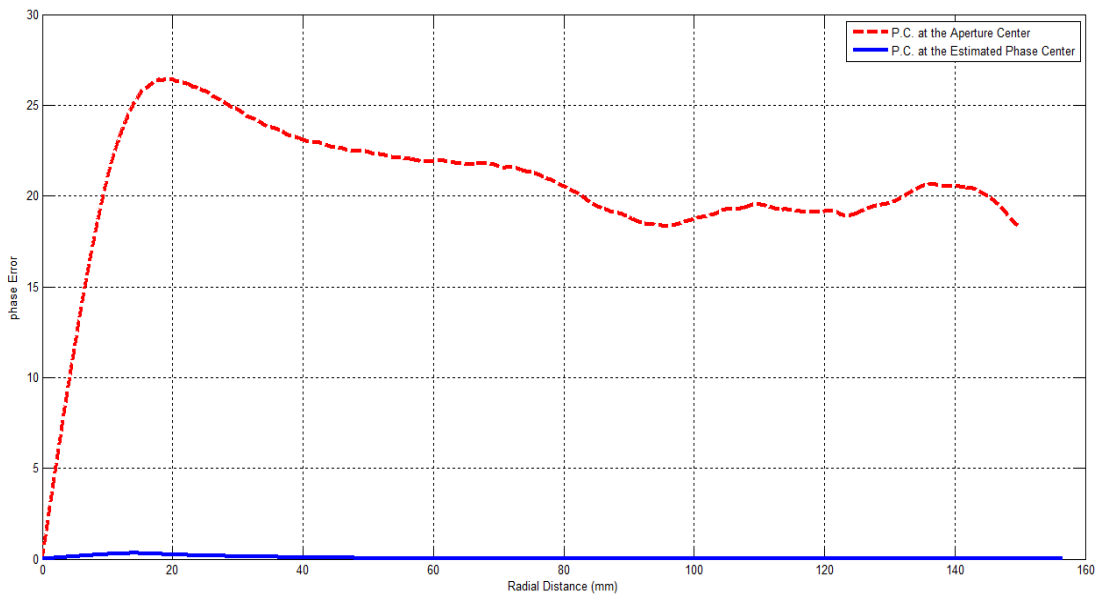


Figure 3.17: The phase errors versus the radial distance for $W_A = 29.19\text{mm}$ aperture

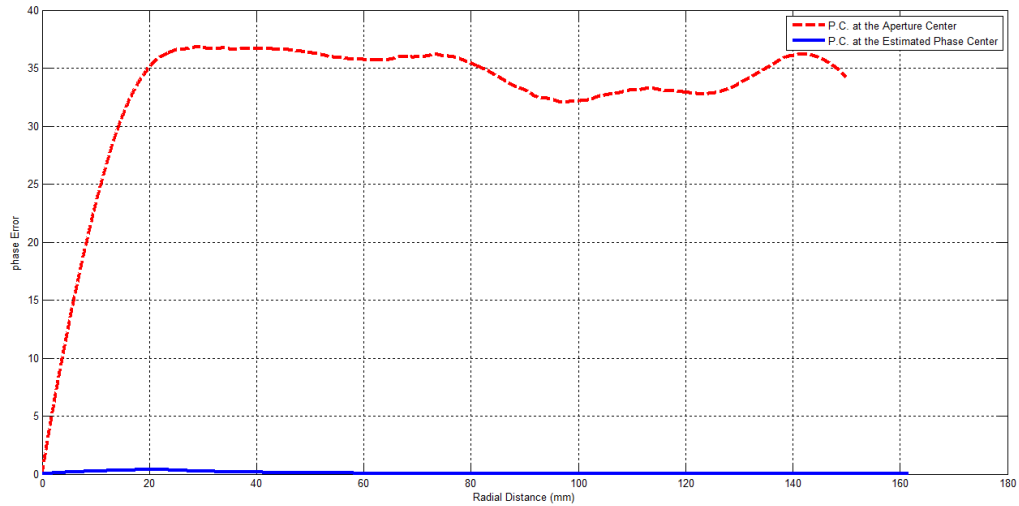


Figure 3.18: The phase errors versus the radial distance for $W_A = 43.785$ mm

Figure 3.16, Figure 3.17 and Figure 3.18 were obtained along the parallel plate at certain distance R by considering the position of the phase center positions in two cases. These figures show the behavior of the phase error along certain distances in the parallel plate region from both of the center of the aperture and the estimated phase center to the ideal phase front and computed phase front respectively.

It can be observed that the phase deviates significantly from the phase at the broadside. These results clearly indicate that the phase center should be at a distant from the aperture center. It is possible using other distance and angles for R and θ to obtain the phase error at near or far field.

Notice that there is a variation in the phase center position according to the type and widths of the radiator. The difference between the results of multi-sections transition radiator and linear taper radiator that have the same aperture width were listed in Table 3.3.

Table 3.3: Comparison of the phase center position for multi-section and linear taper transitions

W_A	The multi-section Transition		The linear taper	
	Δ	x_c	Δ	x_c
17.78mm	2.38mm	4.894mm	2.41mm	4.94mm
29.19mm	3.369mm	6.97mm	3.525mm	7.304mm
43.785	5.466mm	10.6mm	8.12mm	13.85mm

Table 3.3 shows that the multisection transition with this estimated phase center calculation has higher performance compared with the standard taper transition. When the step transition is used the phase center is closer to aperture center, which means less phase errors. Application of the estimation formula results with minimal phase errors.

A study also has been carried out to examine the phase performance of the multi-section transition and the linear taper transition at various frequencies. Figure 3.20 and Figure 3.21 show the phase errors of multi-section transition and linear taper with the same $W_A = \frac{\lambda}{2}$ aperture widths for two phase centers at $f=2\text{GHz}$, 2.45GHz and 3GHz .

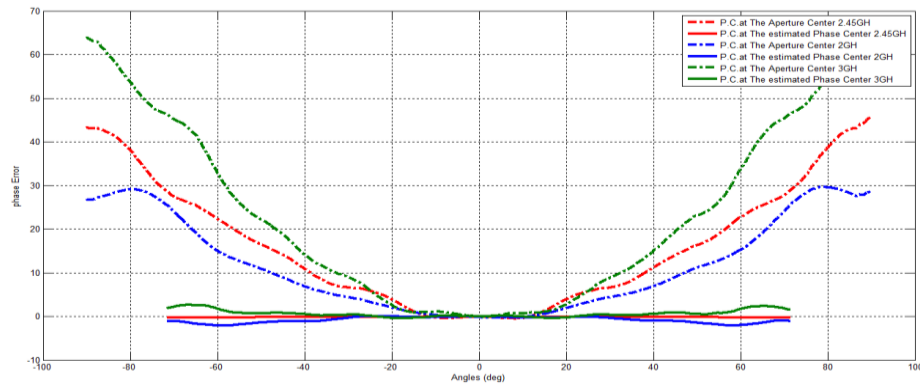


Figure 3.20: The phase errors of $W_A = 29.19$ mm multi-section transition for the two phase centers at 2GHz , 2.45GHz and 3GHz

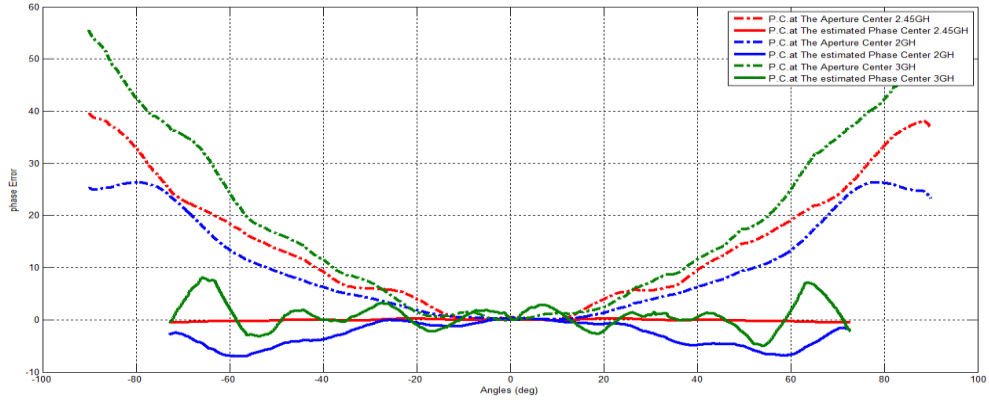


Figure 3.21: The phase errors of $W_A = 29.19$ mm linear taper for the two phase centers at 2GHz, 2.45GHz and 3GHz

The phase error for length designed at 2.45GHz which is 0.38λ for $f=2$ GHz, 2.45GHz and 3GHz. At the design frequency and band of frequencies the phase errors of the multi-section transition are less for the estimated phase error points than the phase errors of the linear taper for the same band of frequency.

Figure 3.22 and Figure 3.23 show the phase errors of multi-section transition and linear taper with the same lengths for $W_A = \frac{3\lambda}{4}$ aperture width for two phase centers at $f=2$ GHz, 2.45GHz and 3GHz. The radiator length is 0.348λ . The length calculated at 2.45GHz.

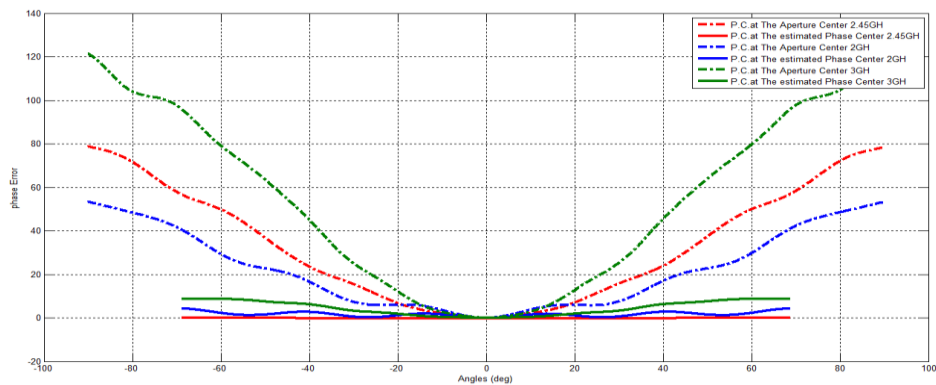


Figure 3.22: The phase errors of $W_A = 43.785$ mm multi-section transition for the two phase centers at 2GHz, 2.45GHz and 3GHz

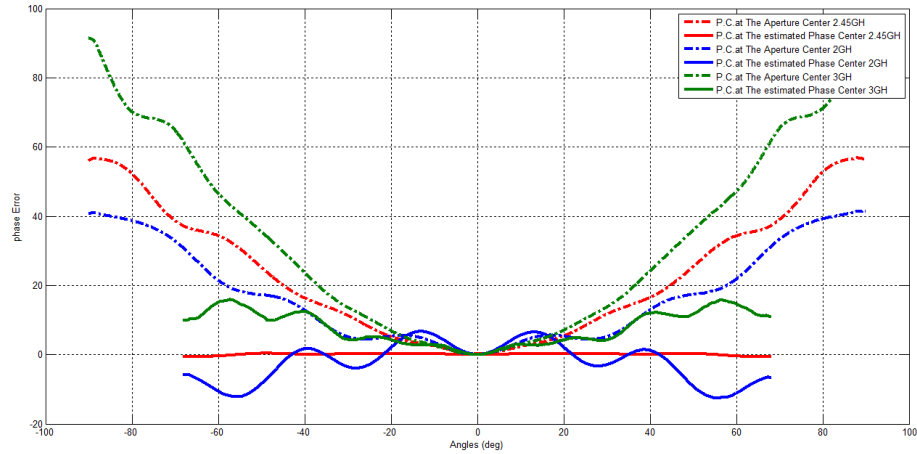


Figure 3.23: The phase errors of $W_A = 43.785$ mm linear taper for the two phase centers at 2GHz, 2.45GHz and 3GHz

The previous results show that the phase errors vary by a very small amount with frequency for the estimated phase center of multi-section transition, while the phase errors of the linear taper vary by larger amount with frequencies than the multi-section transition. On the other hand the results which have been evaluated by using full wave simulation software show that there is almost no change in the position of the phase center for multi-section transition compared to linear taper transition at band of frequencies. Even with larger change in the estimated phase center for linear taper at larger and lower frequencies is no significant change in the position of the estimated phase center.

Figure 3.24 show the comparison of the phase error of the estimated phase center for $W_A = 43.785$ mm aperture width of the linear taper transition and the multi-section transition at $R+x_c$.

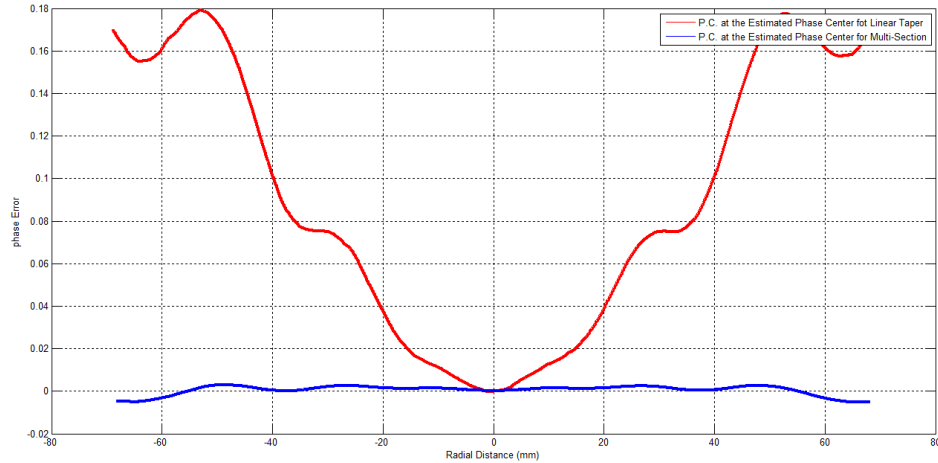


Figure 3.24: The phase errors of $W_A = 43.785$ mm for linear taper and multi-section transitions at the estimated phase center position for 2.45GHz

The comparison of the phase error of the estimated phase center for the linear taper and the multi-section transitions having the same length and width shows that the phase error is very close to zero for the multi-section transition than the phase error at the estimated phase center position for the linear taper.

According to the simulation results of the multi-section transition and the linear taper transition designs, it is clear that the multi-section transition has very high performance and lower phase error compared to the linear taper having the same length and width.

Chapter 4

CONCLUSION AND FUTURE WORK

4.1 Conclusion

A microstrip transitions method by using commercially available simulation software has been used to design transitions between microstrip lines and parallel plate regions at the design frequency. The multi-sections transitions are then used to introduce a method for estimating the phase center of two dimensional radiators, which is essential for Rotman lens applications. A numerical study has been carried out to show the effectiveness of the method. The full wave simulation software has been used for this purpose. The phase center is estimated by equating the phase at two angles and a certain distance from the aperture. The results show that the phase center obtained for three different multi-sections transition widths by this method has very low phase error at the far field.

4.1 Future Work

A new method may be used to obtain the position of the phase centers of the transitions between microstrip lines and the Rotman lens ports. In order to reduce phase errors.

REFERENCES

- [1] Rotman, W., & Turner, R. F. (1963). Wide-angle microwave lens for line source applications. *Antennas and Propagation, IEEE Transactions on*, 11(6), 623-632.
- [2] Archer, D. H., & Maybell, M. J. (2005, July). Rotman lens development history at Raytheon electronic warfare systems 1967-1995. In *Antennas and Propagation Society International Symposium*, (2), 31-34.
- [3] Archer, D. H. (1984). Lens-fed multiple beam arrays. *Microwave Journal*, 27,171.
- [4] Hall, P. S., & Vetterlein, S. J. (1990, October). Review of radio frequency beamforming techniques for scanned and multiple beam antennas. In *Microwaves, antennas and propagation, proc. Inst. Elec. Eng.* 137(5), 293-303.
- [5] Fong, K. S., & Smith, M. S. (1984). A microstrip multiple beam forming lens. *Radio and Electronic Engineer*, 54(7.8), 318-320.
- [6] Smith, S., & Fong, K. S. (1983). Amplitude performance of Ruze and Rotman lenses. *Radio and Electronic Engineer*, 53(9), 329-336.
- [7] Uyguroğlu, R., & Niazi, A. Y. (1999). Designing microstrip transitions into parallel-plate regions using the FDTD method. *Microwave and Optical Technology Letters*, 22(1), 81-84.

- [8] Collin, R. E. (2007). *Foundations for microwave engineering*. John Wiley&Sons.
- [9] Cruz, J. L., Gimeno, B., Navarro, E. A., & Such, V. (1994). The phase center position of a microstrip horn radiating in an infinite parallel-plate waveguide. *Antennas and Propagation, IEEE Transactions on*, 42(8), 1185-1188.
- [10] Pozar, D. M. (2009). *Microwave engineering*. John Wiley & Sons.
- [11] Cheng, D. K. (1993). *Fundamentals of engineering electromagnetics*.